Horizon 2020

Societies of Symbiotic Robot-Plant Bio-Hybrids as Social Architectural Artifacts

Deliverable D2.4

Final report on the development of a bio-hybrid superorganism

Date of preparation: 2019/03/31	**Revision: 1**
Start date of project: 2015/04/01	**Duration: 48 months**
Project coordinator: UzL	**Classification: public**
Partners:	
lead: **AMU**	*contribution:* **UzL, UNIGRAZ, CITA, ITU, CYB**
Project website:	http://florarobotica.eu/

H2020-FETPROACT-2014

DELIVERABLE SUMMARY SHEET

Grant agreement number:	640959
Project acronym:	*flora robotica*
Title:	Societies of Symbiotic Robot-Plant Bio-Hybrids as Social Architectural Artifacts

Deliverable N^o:	Deliverable D2.4
Due date:	M48
Delivery date:	2019/03/31

Name:	**Final report on the development of a bio-hybrid superorganism**
Description:	Final report of the control methods and the investigated approaches to guide plant growth in order to create a biohybrid system of the two cooperating agent groups: plants and robots.

Partners owning:	**AMU**
Partners contributed:	**UzL, UNIGRAZ, CITA, ITU, CYB**
Made available to:	public

Contents

1 Introduction

Figure 1: The *flora robotica* bio-hybrid system: robotic node (2nd generation, see chapter 2 for 3rd generation) and bean plants.

This is the final report of work package two called 'Becoming.' We present our results on algorithms for the growth of bio-hybrids combining biological and artificial components (see Fig. 1). The bio-hybrid structures that we grow in *flora robotica* can arguably be called 'superorganisms.' If "groups and communities can possess similar properties of functional organization," then we regard them as superorganism [10]. The idea of superorganisms in biology is rather old but was revived especially in the context of honeybee research [7, 10]. The concept is, however, open to any organism and Wilson and Sober [10] even mention a suggested plant experiment in their paper. Carrapiço [2] identifies ecological behaviors in Azolla (an aquatic fern) in cooperation with microorganisms. Sanders [6] speaks of a superorganism in fungal and algal growth. The superorganism concept was not explicitly investigated in *flora robotica* but our robotic nodes form a decentralized, self-organizing system (requirement for swarm intelligence) and they closely interact with a group of plants. The plants, in turn, react to the stimuli triggered by the robots, hence, help to form a 'functional organization.'

An algorithm for autonomous bio-hybrid growth provides clearly defined steps that allow for the efficient design of plant-robot bio-hybrids and it is implemented in *flora robotica*'s demonstrator of a bio-hybrid system. The algorithm controls complex plant and robot behaviors as required for the 'becoming' of a bio-hybrid triggering the growth and form of desired shapes.

One main challenge of this project was to consolidate two worlds of scientific experiment: plant science and robotics. In chapter 2 we present our experiment protocol of steered bio-hybrid growth. We extend the variety of possible shapes by adding the functionality of repelling growth (see Sec. 3.2).

Chapter 4 is committed to applications of measuring *in planta* electric potentials and its utility in *flora robotica*'s bio-hybrids. The extensive data analysis was done to study differences in phytosensing data in response to light of various colors. Moreover, interesting results about the possibilities of detecting *in planta* cutting plant organs are presented. Preliminary plant 'training' effects based on phytosensing may have consequences in future bio-hybrid developments and even in plant science.

Chapter 5 is dedicated to the Vascular Morphogenesis Controller (VMC). We investigate a variety of possible structures generated and controlled by VMC and analyze decision-making in self-assembly processes using VMC. The potential of VMC is described in detail and the corresponding hardware implementations are presented in deliverable D3.3.

2 Algorithm for autonomous bio-hybrid growth

In previous deliverables we have reported a first generation of robots for plant shaping via light stimuli, tested in a small set of experiments lasting up to seven weeks. New experiments and a new generation of robot development are presented in *D1.4 Evaluation of the robotic symbiont*. We have also established a more generalized protocol for this type of plant-robot experiment, which we are in the process of making publicly available as a resource (paper conditionally accepted [9]). Here are reported the software and setup sections of our generalized open-source protocol, with examples given in images of the final generation setup. The robot hardware section is reported in *D1.4 Evaluation of the robotic symbiont*.

The protocol reported here is for the basic approach (i.e., using only attractive stimuli). Extensions to repelling stimuli are handled in the following section.

2.1 Generalized open-source protocol

2.1.1. Robot control for bio-hybrid shaping

Robot Control:

Step 1. During each experiment, run the software protocol on each robot in parallel, enabling their autonomous behavior.

Step 2. Establish two possible states for the robot (see Fig. 2):

(a) A 'stimulus' state during which the robot emits blue light at the required intensity.

(b) A 'dormant' state during which the robot either emits no light or emits red light.

Step 3. Depending on the experiment type, give the appropriate predefined information. In control and single-decision experiments, assign each robot a state to continuously execute. In multiple-decision experiments, supply to each robot a full configuration map of the pattern of plant growth to be tested in the current experiment.

Step 4. In multiple-decision experiments, run the 'Initialization' process, as follows.

(a) Set the location of the robot within the setup.

(b) Compare the robot's location to the supplied map. If the robot's location is the first location on the map, set the robot to 'stimulus;' otherwise, set the robot to 'dormant.'

(c) 'Initialization' process ends.

Step 5. In multiple-decision experiments, run the 'Steering' process, as follows. Execute iteratively.

(a) Check the robot's IR-proximity sensor reading to see if a plant has been detected.

(b) If a plant is detected and the robot is set to 'dormant,' then maintain.

(c) If a plant is detected and the robot is set to 'stimulus,' then:

(i) Notify the adjacent neighboring robots that a plant has been detected, and include the robot's location in the message.

(ii) Set the robot to 'dormant.'

(iii) Compare the robot's location to the map. If the robot is at the last location on the map, then send a signal over WLAN that the experiment is complete.

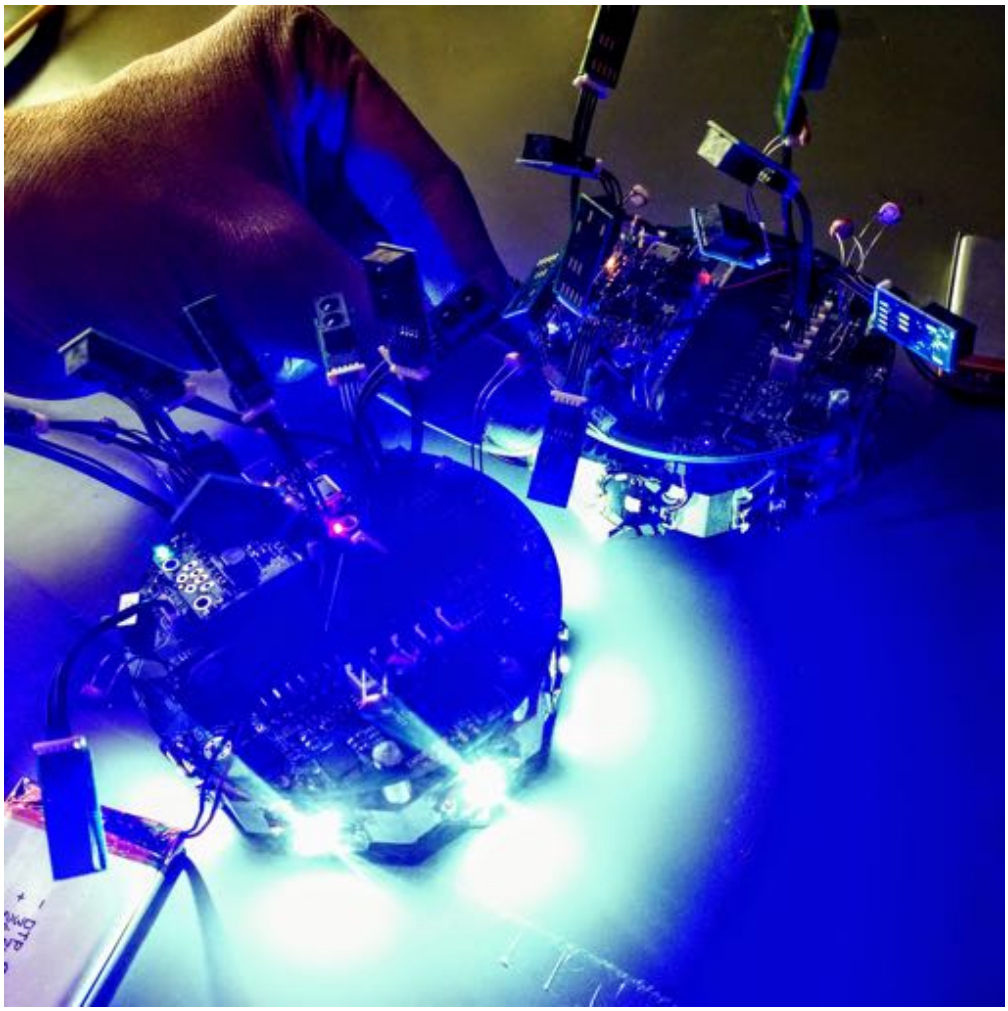

Figure 2: Two unenclosed robotic nodes of the final generation, with the left node set to 'stimulus' and the right node set to 'dormant.'

(d) Check the robot's incoming messages from its adjacent neighboring robots to see if one of them that was set to 'stimulus' has detected a plant.

(e) If a 'stimulus' neighbor has detected a plant, compare that neighbor's location to the robot's location, and also compare to the map.

(f) If the robot is at the subsequent location on the map, set the robot to 'stimulus.'

(g) End the iterative loop of the 'Steering' process once a signal has been received that the experiment is complete.

2.1.2. Context: lab conditions and experiment setup

Experiment Design:

Step 1. Place robots and mechanical supports in a grid large enough to cover the growth

area and pattern being tested in the experiment. The minimum setup includes one row and two columns of robots.

Step 2. Below the bottom row of robots, place a row of the standard diagonal mechanical supports, matching those throughout the setup. Where the lower ends of these supports intersect, join them mechanically with a 'y-joint.' For each 'y-joint' at the base of the setup, plant a uniform number of plants according to the size of the diagonal grid cell (roughly one plant per 10 cm of exposed mechanical support length), with the plant health maintenance conditions described above.

Step 3. Experiment setup. Select an experiment type to run, and where relevant select a quantity and distribution of robots.

(a) **Experiment type 1: Control.** This experiment type tests growth of the climbing plants in conditions absent of light stimuli to trigger phototropism. It can run on any size and shape of setup. In Step 3 of the robot control protocol, assign all robots the 'dormant' state and run continuously until results are manually assessed to be complete. In a successful experiment, none of the plants will find or attach to the mechanical supports.

(b) **Experiment type 2: Single decision.** This experiment type tests the plants' growth trajectories when presented with binary options—one support leading to a 'dormant' robot and one support leading to a 'stimulus' robot. It runs only on the minimum setup (i.e., one row, two columns). In Step 3 of the robot control protocol, assign one robot the 'dormant' state and one robot the 'stimulus' state. Run continuously until one of the two robots detects a plant with the IR-proximity sensor. In a successful experiment, the robot with the 'stimulus' state will detect a plant after it had grown along the respective support.

(c) **Experiment type 3: Multiple decisions.** This experiment type tests the plants' growth when presented with multiple subsequent stimuli conditions, that trigger a series of decisions according to a predefined global map. It can run on any size and shape of setup that has more than the minimum number of rows (i.e., two or more). In Step 3 of the robot control protocol, provide a global map of the pattern to be grown. Then execute Step 4 and 5. In a successful experiment, at least one plant will have grown on each support present in the global map. Additionally, no plant will have chosen the incorrect direction when its growing tip is located at the currently active decision point. (To clarify, extraneous growing tips are not considered here, if for instance a branching event places a new growing tip at an obsolete location on the map.)

Plant Species Selection Procedure:

Step 1: Plant species selection. This protocol focuses on the plant behaviors related to climbing, directional responses to light, and the health and survival of the plants in the specific season, location, and experimental conditions. (An example species meeting the selection criteria is the climbing common bean, *P. vulgaris*.)

(a) Select a flowering species known to display strong positive phototropism towards UV-A and blue light (340–500 nm) in the growing tips. This will mean that, in the selected species, the phototropins (light-receptor proteins) in the plant will absorb photons corresponding to wavelengths 340–500 nm. When the receptors are triggered, first swelling will occur in the stem by the preferential relocation of water to the stem tissues opposing the triggered receptors, causing a reversible directional response. Then, within

the stem auxin (plant patterning hormone) is directed to the same tissue location, perpetuating the directional response and fixing stem tissues as they stiffen.

(b) Select a species that is a winder, in which the circumnutation behavior is pronounced and the growing tip has helical trajectories with large enough amplitude to wind around the mechanical supports used in the specific experimental conditions. The twining behavior exhibited by the selected winder should tolerate the environment and nutrient conditions present in the experiment, and should tolerate mechanical supports with angle of inclination up to 45°.

(c) Select a species that will grow reliably and quickly in the experimental conditions, with an average growth speed not less than approximately 5 cm per day, and preferably faster if possible.

(d) Select a species that will display the required behaviors in the present season and geographic location.

Step 2. Ensure the species tolerates the range of environmental parameters that will be present in the experimental setup. The plant should tolerate an absence of green light and an absence of light outside the visible spectrum (400–700 nm), as in the setup the plants will be exposed only to isolated blue light and isolated red light. The phototropism reaction in the plant will respond to light from blue diodes with peak emission $\lambda_{\max} = 465$ nm, and photosynthesis in the plant will be supported by red diodes with peak emission $\lambda_{\max} = 650$ nm. The plant should also tolerate any present fluctuations in temperature, kept at approximately 27°C, as well as any present fluctuations in humidity and watering.

Plant Health Monitoring and Maintenance Procedure:

Step 1. Locate the experiment setup in controlled environmental conditions—i.e., indoor with no incident daylight or other light external to the conditions described below, with controlled air temperature and humidity, and with controlled soil watering. Monitor the conditions with sensors that are connected to a microcontroller or single-board computer that is WLAN enabled.

Step 2. Maintain plant photosynthesis using LED growth lamps external to the robots and facing the experiment setup. The growth lamps should deliver monochromatic red light to the setup, with red diodes having peak emission at approximately $\lambda_{\max} = 625$–650 nm, with no critical wavelengths outside the range 550–700 nm, except for a low incidence of ambient blue light if helpful for the health of the selected species. (If a low incidence of ambient blue light is included, restrict to levels at a very minor fraction of those emitted by a single robot, see Fig. 3.) If using lamps that include LEDs of a color other than red, obstruct those. Provide the levels of red light required for the health of the selected species, for instance for *P. vulgaris* provide roughly 2000 lumens or more in total. Orient the growth lamps to face the experiment setup, such that their emittance is distributed roughly evenly over the growth area. Monitor the ambient light conditions using an RGB color sensor.

Step 3. After germinating, provide each plant its own pot at the base of the experiment setup. Provide suitable soil volume and type for the selected species, for example roughly 3 l of commercial gardening soil per pot for *P. vulgaris* that will grow to several meters in height. Ensure the soil and seeds have been sanitized prior to germination. If needed, use suitable pest control methods to prevent or manage insects.

Step 4. Regulate air temperature and humidity levels, accordingly for the selected species

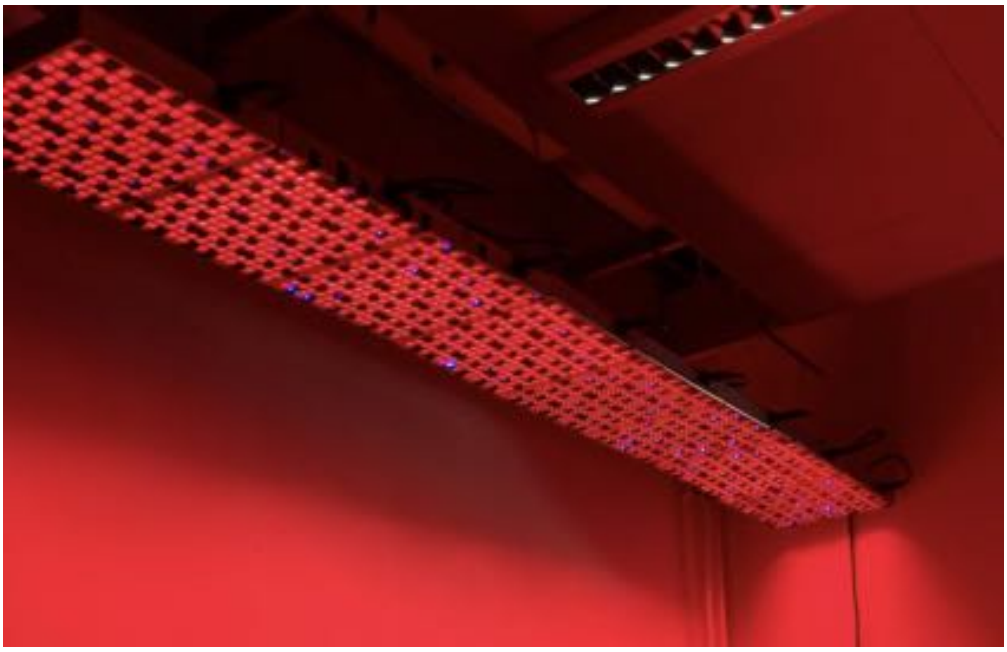

Figure 3: Growth lamp setup in lab for delivering red light. Off-the-shelf lamps with blue LEDs obstructed to limit them to minor incidence.

(e.g., a temperature of 27°C for *P. vulgaris*). Monitor levels using a temperature-pressure-humidity sensor. Levels can be maintained using heaters, air conditioners, humidifiers, and dehumidifiers.

Step 5. Monitor the soil using a soil moisture sensor, and maintain an appropriate rate of watering for the selected species. This can be executed using an automated watering system where water is delivered to the soil via nozzles as triggered by the soil moisture sensor readings (see Fig. 4). Alternatively, the soil can be watered manually, as regulated by the sensor readings.

Recording Procedure:

Step 1. Store data (from sensors and cameras) initially at the single-board computer where the data has been generated onboard. Run onboard reply servers that respond to needed requests, such as the last stored sensor reading. At regular intervals upload the data and log files over WLAN to a local network-attached storage (NAS) device.

Step 2. Capture time-lapse videos of the experiments continuously using cameras positioned at two or more vantage points, with at least one camera view encompassing the full experiment setup. Ensure the captured images are of high enough resolution to adequately capture the movements of the plant growing tips, typically only a few millimeters in width. Automate the image capture process to ensure consistent time intervals between captures, using either an onboard camera on a single-board computer, or a stand-alone digital camera automated with an intervalometer or similar. Install lamps to act as flashes, automated similarly to the cameras. Ensure the flashes are bright enough to compete with the red light of the growth lamps without dramatically post-processing the images for color correction. Locate

Figure 4: Lab setup of automatic watering system, with *P. vulgaris* germinated in individual pots at the base of the experiment setup.

the flashes such that the experiment setup can be fully illuminated and therefore clearly visible in images. Synchronize the cameras and the flashes such that all cameras capture images simultaneously, during a 2 s flash period. Capture the images every 2 minutes, for the duration of each experiment.

Step 3. Log the environmental sensor data, specifically the readings from the temperature-pressure-humidity sensor, the RGB color sensor, and the soil moisture sensor. Log the data from all robots in the setup, specifically the IR-proximity sensor and photoresistor readings, as well as the internal state of the robot which defines its LED emittance status.

Step 4. Make all recorded data available for remote monitoring of the experiments, via regular real-time reports (see Fig. 5) or visualizations, to ensure correct conditions are maintained for the full duration of a potentially months-long experiment.

2.2 Implications for bio-hybrids and plant-robot experiments

Congruent with the increasing prevalence of automation in manufacturing and production, robots are being utilized to sow, treat, and harvest plants. We use robot technology to automate plant experiments in a non-invasive manner, with the purpose of steering growth via directional responses to stimuli. Traditional gardening practices have included the manual shaping of trees and bushes by mechanical restraint and cutting (see Fig. 6). We present a methodology that can for instance be applied to this shaping task, by steering growth patterns with stimuli. Our presented methodology is also a step towards automated plant experiments, with a specific focus on providing light stimuli. Once the technology has become robust and reliable, this approach has potential to reduce costs in plant experiments and to allow for new automated experiments that would otherwise be infeasible due to overhead in time and manual labor. The robotic elements are freely programmable and act autonomously as they are equipped with sensors, actuators for stimuli provision, and microprocessors. While we focus on proximity sensing (i.e., measuring distances at close-range) and light stimuli, many other options are feasible. For example, sensors can

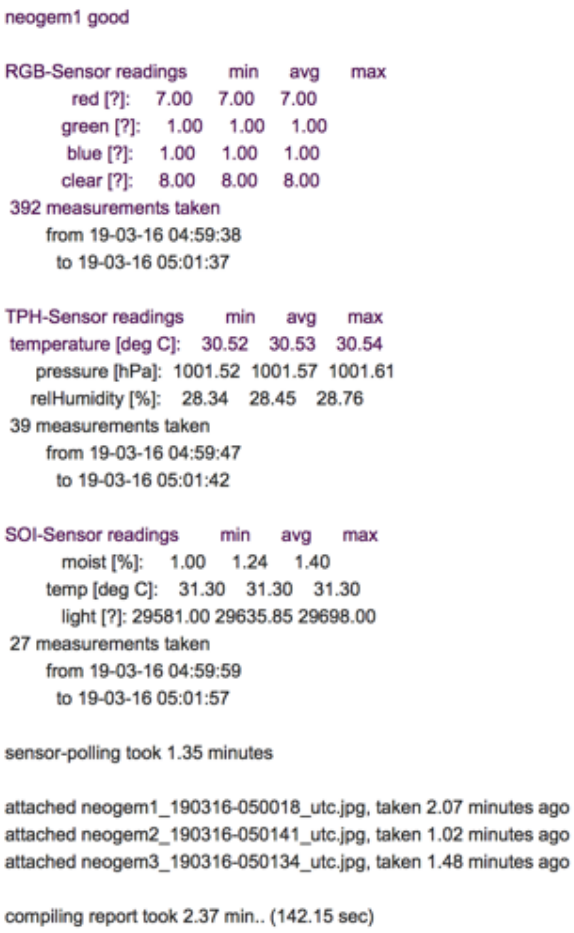

Figure 5: Screen capture of example hourly email report for remote experiment monitoring.

be used to analyze plant color, to monitor biochemical activity, or for phytosensing approaches to monitor for instance environmental conditions through plant electrophysiology. Similarly, actuator options might provide other types of stimuli, through vibration motors, spraying devices, heaters, fans, shading devices, or manipulators for directed physical contact. Additional actuation strategies (see fabrication and steering of braided mechanical scaffolds in D1.4 and D3.3) could be implemented to provide slow mobility to the robots (i.e., 'slow bots' [1]), such that they could gradually change the position and direction from which they provide stimuli. Furthermore, as the robots are equipped with single-board computers, they could run more sophisticated processes such as visioning for plant phenotyping or artificial neural network controllers for stimuli actuation (as previously reported in D2.3). As the plant science research focus is often on early growth (i.e., in shoots), the whole domain of using autonomous robot systems to influence plants over longer periods seems underexplored and may offer many future opportunities. Going even one step further, the robotic elements can be seen as objects of research themselves, allowing the study of the complex dynamics of bio-hybrid systems formed by robots and plants closely interacting. The robots selectively impose stimuli on the plants, the plants react according to

their adaptive behavior and change their growth pattern, which is subsequently detected by the robots via their sensors. Our approach closes the behavioral feedback loop between the plants and the robots and creates a homeostatic control loop.

(a) (b)

Figure 6: Images from our *flora robotica* site visit to UK firm Full Grown (https://fullgrown.co.uk). Traditional manual shaping processes to grow plants into furniture, which could be automated or semi-automated by a future development of our robotic nodes for plant shaping.

The presented methodology shows initial steps toward automating the stimuli-driven steering of plant growth, to generate specific patterns. This requires continuous maintenance of plant health, while combining into a single experiment setup the distinct realms of biochemical growth responses and engineered mechatronic functions—sensing, communication, and controlled generation of stimuli. As our focus here is on climbing plants, mechanical support is also integral.

A limitation of the current setup is its scale but we believe our methodology easily scales. The mechanical scaffold can be extended for larger setups and therefore longer periods of growth, which also allows expanded configurations and patterns. Here the setup is limited to two dimensions and binary left-right decisions, as growth is limited to a grid of mechanical supports at 45°inclination, and plant decision positions are limited to that grid's bifurcations. Mechanical extensions may include 3D scaffolds and differing materials, to allow for complex shapes.

The methodology can be considered as a system to automatically grow patterns defined by a user. By extending the possible complexity of mechanical configurations, users should face few restrictions on their desired patterns. For such an application, a user software tool should confirm that the pattern is producible, and the mechatronics should then self-organize the production of the pattern by generating appropriate stimuli to steer the plants. The software should also be extended to include recovery plans and policies determining how to continue with the growth

if the original planned pattern has partially failed—for instance if the first activated robot has never detected a plant but the dormant ones have seen that the position of the growing tips are beyond the activated robot.

The current setup focuses on light as an attraction stimulus. If the desired pattern requires a separation between different groups of plants—e.g., the desired pattern needs two groups of plants to choose opposite sides—then it may not be feasible using only one type of stimulus. For such complex growth patterns independent of scaffold shape, the different groups of plants can potentially be grown in different time periods such that their respective attraction stimuli do not interfere, which would also allow the integration of branching events. However this may not always be a suitable solution, and the standard attractive light stimulus could then be augmented by repelling influences such as shading, or by other stimuli like far-red light or vibration motors.

The method and the experiment design are a step towards a sophisticated methodology to automatically influence directional growth of plants. The experiment setup is basic by determining only a sequence of binary decisions in the plants and we focus on one, easy to manage stimulus. Additional studies would be required to prove the method's statistical significance, to add more stimuli, and to control other processes such as branching. With sufficient development to guarantee the long-term reliability of the robots, the presented methodology could allow for automation of plant experiments over long time periods, reducing the overhead associated with the study of plant development stages beyond that of shoots. Similar methods can allow for future investigations into the underexplored dynamics between biological organisms and autonomous robots, when the two act as tightly coupled self-organizing bio-hybrid systems.

3 Supplementing autonomous shaping in bio-hybrids by growth repelling

3.1 Extending control protocol to growth repelling

The basic approach for bio-hybrid plant shaping can be extended to achieve greater flexibility in patterns by supplementing the attractive stimulus with a repelling stimulus. Multiple repelling stimuli are candidates (see below), and can be substituted within the same hardware platform, as the final generation of robotic nodes are extensible via external modules that can be powered and controlled by the main robotic node (see *D1.4 Evaluation of the robotic symbiont*). Here are reported the revisions to the robot control protocol above for a setup that includes repelling extension modules. Steps 2, 4, and 5 of the control protocol contain revisions for such an extension.

Step 1. *No change.*

Step 2. Establish three possible states for the robot:

(a) A 'stimulus A' state during which the robot emits blue light at the required intensity.

(b) A 'stimulus B' state during which the robot directs its extension module to deliver the repelling stimulus.

(c) A 'dormant' state during which neither the robot nor its extension module deliver a stimulus that impact directional growth.

Step 3. *No change.*

Step 4. In multiple-decision experiments, run the 'Initialization' process, as follows.

(a) Set the location of the robot within the setup.

(b) Compare the robot's location to the supplied map. If the robot's location is the first location on the 'growth' map, set the robot to 'stimulus A.'

(c) Otherwise, compare the robot's location to the negative zones of the map (i.e., the 'no growth' zones). If the robot's location is within the 'no growth' zones AND within radius r (where r is the distance within which the repelling stimulus is effective) of the height in line with the map's base, set the robot to 'stimulus B.'

(d) otherwise, set the robot to 'dormant.'

(e) 'Initialization' process ends.

Step 5. In multiple-decision experiments, run the 'Steering' process, as follows. Execute iteratively.

(a) Check the robot's IR-proximity sensor reading to see if a plant has been detected.

(b) If a plant is detected, always notify the adjacent neighboring robots that a plant has been detected, and include the robot's location in the message.

(c) If a plant is detected and the robot is set to 'dormant' or to 'stimulus B,' then maintain state.

(d) If a plant is detected and the robot is set to 'stimulus A,' then:

(i) Set the robot to 'dormant.'

(ii) Compare the robot's location to the 'growth' map. If the robot is at the last location on the map, then send a signal over WLAN that the experiment is complete.

(e) Check the robot's incoming messages from its adjacent neighboring robots to see if one of them has detected a plant.

(f) If a neighbor has detected a plant, then:

  (i) Compare that neighbor's location to the robot's location, and also compare to the 'growth' map.

  (ii) If the neighbor is set to 'stimulus A' AND the robot is at the subsequent location on the 'growth' map after the neighbor, set the robot to 'stimulus A.'

  (iii) Otherwise, if the robot is within the 'no growth' zones AND the neighbor is within r of the robot, set the robot to 'stimulus B.'

  (iv) Otherwise, maintain state.

(g) End the iterative loop of the 'Steering' process once a signal has been received that the experiment is complete.

3.2 Repelling growth by spraying plant growth inhibitors

In deliverable 2.3 we reported results of investigation on finding appropriate stimulus for inhibiting growth of plants. Blue light is utilized as plant growth stimulator and as trigger of phototropism, that is, redirection of growth towards a blue light source. The usage of TIBA dissolved in lanolin cream (2,3,5triiodobenzoic acid) was shown in D2.3 as effective in decreasing plants growth rate. However, application of TIBA in cream is unfeasible for being robotized and automated, but TIBA is degraded in water in short time, so water solutions are infeasible. Spraying of growth inhibitors was chosen as a more reasonable application considering automation in our application. Having this in mind, we tested commercial growth inhibitors for their effectivity in inhibiting growth of beans. Farmers use them mostly to make rape (*Brassica napus*) more robust and to synchronize flowering. All tested substances are stable in water solution, non-toxic in reasonably small amounts for humans, inexpensive, and easily available on the market. Moreover, they can have additional antifungal effects (for example Toprex and Caryx). We have tested Toprex 375 SC (Syngenta), Fazor 80 SG (Arysta Life Science) and Caryx 240 SL (Bayer) for effect on inhibition of beans growth 7. Beans were sprayed once in water solutions with a simple plant sprayer. Approximately 10 ml were applied per plant. Applied concentrations:

1. 0.4% Fazor 80 SG (Maleic hydrazide)
2. 0.3% Toprex 375 SC (difenokonazol and paklobutrazol)
3. 0.5% Caryx 240 SL (metkonazol and mepikwat chloride)

The treated beans had grown for ten days after germination and close to the phase of the prominent stem elongation. The strongest effect, measured as growth inhibition in comparison to non-treated plants, was observed for Toprex. Beans treated with Toprex grew almost ten times less than non-treated beans: 2.63 cm for Toprex treated vs. 19.65 cm for control plants. No deleterious side effects were observed. A repetition of the experiment with Toprex influence on beans growth resulted in the same outcome. **We choose Toprex as the best 'repellent,' growth inhibitor, that might be used in final bio-hybrid for counteracting fast plants growth rate, which, if being uncontrolled, might make impossible to obtain our desired shapes of architectural artifacts**. Hardware modules for the autonomous utilization of Toprex in bio-hybrids are described in *D1.4 Evaluation of the robotic symbiont*.

3.3 Influence of far-red light on bean growth

Choosing a chemical growth inhibitor for spraying provides us with an efficient tool for inhibiting bean growth. However, we have studied alternatives to inhibit plant growth. The idea of using different light wavelengths not only for redirecting plant growth, but also for inhibiting the growth was considered an option and having potential for being more precisely applied than sprayed chemicals. The clear effect of light intensity on plant growth rates was reported in deliverable D2.3, but there were difficulties to precisely control strong white light. We decided to test effects of far-red light on plant growth, too. Effects of far-red light on plants strongly depends on red:far-red light ratio and consequently phytochrome signaling. Many developmental processes are influenced by phytochrome signaling pathways, for example: flowering, germination, and shade avoidance response.

Red light is used as Photosynthetic Active Radiation and is stable during the day in the *flora robotica* bio-hybrid system. A manipulation with different intensities of far-red light might enable us to influence plant growth. Having in mind the shade avoidance response we expected that far-red light may act as growth inhibitor. As preliminary proof-of-concept experiments, we investigated the influence of constant far-red light in semi-natural light conditions (greenhouse).

Two far-red LED panels were delivered by Cybertronica and tested for their influence on beans growth rate in greenhouse conditions. Each panel (see Fig. 9) consists of 10 far-red LED OSLON SSL 80 GF CS8PM1.24-3S4S-1, 730 nm, $I_F = 350$ mA, $V_F = 1.85$ V mounted with thermally conductive epoxy adhesive on the aluminum profile ($20 \times 80 \times 200\ mm^3$) that acts as heat sink to provide efficient LED cooling and as basement plate for LED mounting. Sunlight was coming mostly from the ceiling and one side of the greenhouse. Additional ceiling light was switched on, on cloudy days. Our relatively strong far-red light source was installed 20 cm above soil with bean seeds. Some beans were exposed to stronger, some to weaker far-red light, depending on their distance to the far-red light source. Five days after germination, the non-treated plants (avg. 22.6 cm, stdev. 3.5 cm, $n = 30$) were similar to the treated plants (avg. 23.7 cm, stdev. 2.1 cm, $n = 30$). Germination rate was high for both the controls and far-red treated beans. We observed no significant difference in the growth rates and plant development. The only observed difference was a one week faster sign of senescence (yellow leaves) of the far-red treated beans, that is, six vs eight weeks.

In the second version of experiment far-red light was installed on the side of growing beans and it also did not make any difference in beans growth rate and growth direction (i.e., no negative or positive phototropism reaction). The more enlighten or more shady side of beans culture was direction of applied far-red also did not make any difference. Also no influence on branching was observed in any experiments with far-red LEDs. Despite that far-red light was shown to influence plants growth and development, our tests on far-red LEDs in greenhouse conditions did not shown any promising results for potential application in bio-hybrid beans growth control.

Figure 7: Example far-red treated (on the bottom) and control plants. Beans were growing in greenhouse with 12 hours day, 12 hours night and constant far-red for stimulated plants. Plants on the image are one week after germination.

Figure 8: Far-red treated plants in the side directed far-red light experiment. Beans were growing in greenhouse with 12 hours day, 12 hours night and constant far-red for treated plants. Two generation of plants in two flowerpots are visible (front black one and behind).

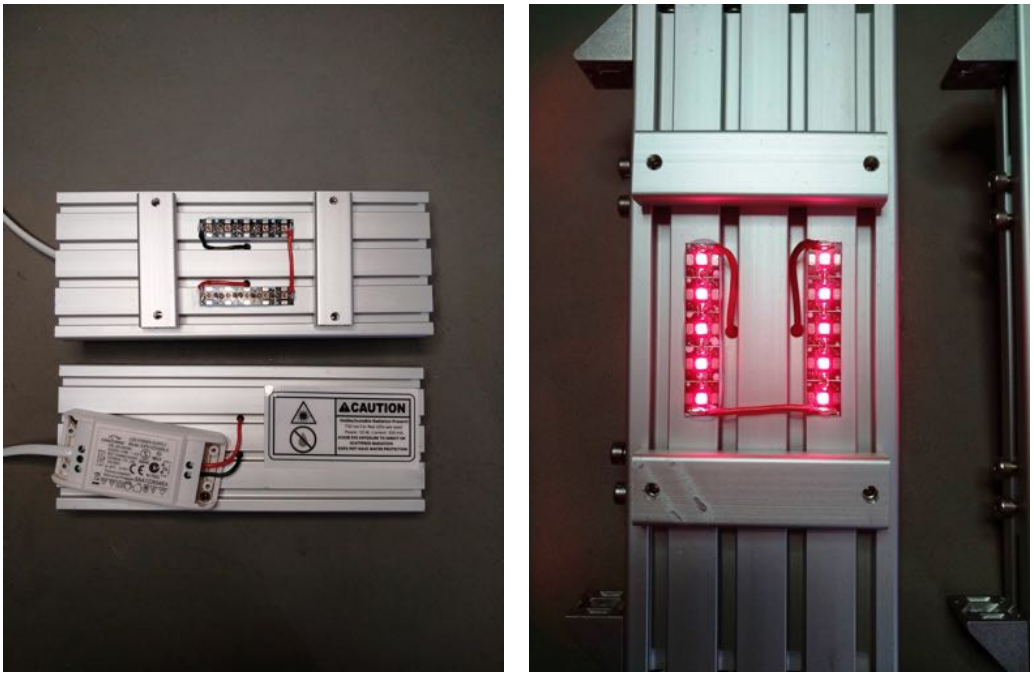

Figure 9: 10 LED 730 nm far-red panel.

4 Phytosensing for the bio-hybrid application

4.1 Data analysis of a plant's electric potential to identify color of light

As reported previously, we use the Phytosensor of CYBRES as tool to monitor plant physiological reactions to environmental factors. As reported in Deliverable 1.3, experiments with *phytosensing* have shown that repetitive mechanical stimulation results in repetitive changes in the electric potential between electrodes inserted in plant stems. However, the results suggested that it may be difficult to distinguish reactions of different types of stimulation, such as touching, shaking, and cutting leaves. In this report we present results on using our Phytosensor to analyze plant electrophysiological reactions to changing light conditions. Light of different colors is used for growth manipulation in our *flora robotica* bio-hybrids.

Understanding plant electrical signaling is a great challenge, mostly because of the lack of methods and models, that may prove to be as useful as in the case of animals. Recently, updates on methodologies have been reported for both electrophysiological data analysis and the design of experiments to reveal signal propagation mechanisms [8, 5]. Also machine learning techniques were found to be useful in the classification of abiotic stresses in plants, such as salt and drought [5]. It is one of our most successful approach for plant sensing besides other investigations in *flora robotica*. Not applicable here are too specialized methods, such as stomata electrophysiology.

Electrodes were inserted into stems of 14 DAG (Days After Germination) tobacco (*Nicotiana benthamiana*) and 20 DAG tomato plants (*Lycopersicon esculentum*) with a 3 cm distance between the electrodes. The Phytosensor was collecting data of electric potentials every 11 seconds, in average 110 reads every 20 minutes, 330 reads every hour, 7,920 reads daily. Note that long term measurements are costly and not many repetitions can be done, also due to unwanted and unpredictable terminations of the Phytosensor after a few days in operation. However, in *flora robotica* we are mostly interested in short time plant reactions to stimuli and as reinforcement of a bio-hybrid's action. For data analysis we chose ten datasets that were collected in five experiments, four conducted on tobacco, and one on tomato.

Plants were cultivated in stable temperature with regular, short-time changes in the light conditions (red, green, blue, and optionally no light: 20 min interval for each light color phase; NeoPixel 144 LEDs strip). We assume that for *flora robotica* natural circadian changes are of less important and we are more interested in short term plant reaction to changing light wavelengths. This is relevant when robotic nodes dedicated to plant shaping switch to different light colors or switch their lights on and off within seconds. The change in the light wavelength is rapid and discrete. The developed data analysis software tool uses several Python packages, such as Pandas, Numpy, Matplotlib, Statsmodels, and Sklearn.

Plots of electric potential data show similar issues as before, as they are usually lacking a clear, stable trend. An analysis was performed on two different scales of data: from 50,000 to over 100,000 sensor readings, and also batches of 2,000 reads. Signals generally were constantly fluctuating in a range of a few thousand micro-volts, that seems to be caused by plant cells and apoplast changes in ion concentrations and subsequent biopotential changes, see Fig. 10. We failed to assign irregularly occurring outliers to specific time or any environmental change. A cause for datasets with biases or rapid shifts in their potential level (up to 10,000 μV) may be unstably inserted electrodes. Support for this hypothesis is that biases and shifts occurred in only one out of two plants that were simultaneously measured. Plots of parts of the data with stable potential level showed usually regular peaks with approximately similar frequency and amplitude (see Fig. 10). There was no significant differences in means, medians, and standard deviations of collected data that was grouped by light colors. Calculating differences between

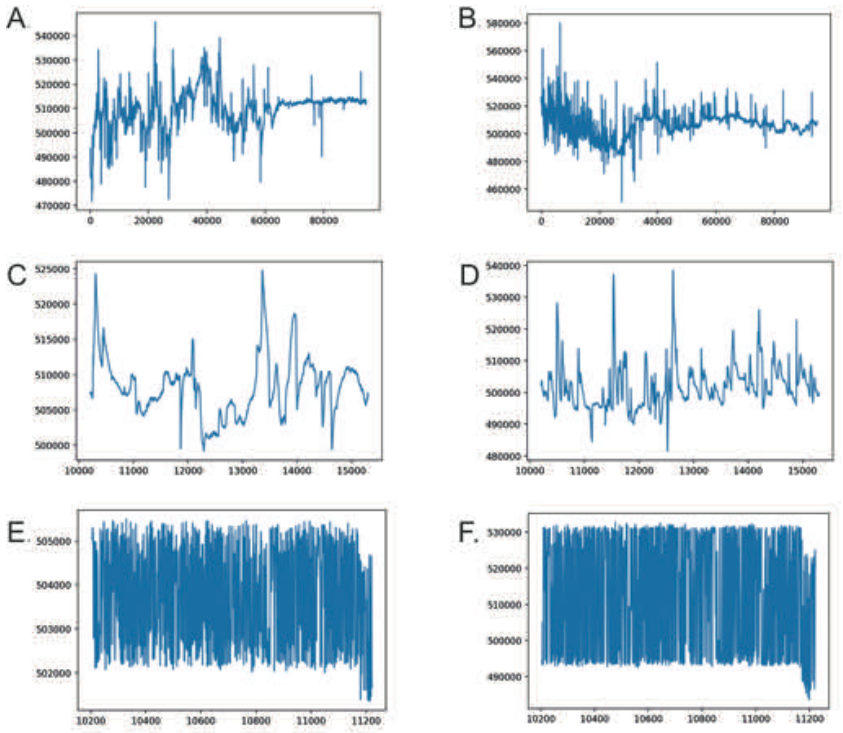

Figure 10: Example plots of plants electric potentials from Phytosensor measurements. Electrodes were inserted into tobacco stems and 20 min. of red, then green, then blue light was applied to plants. One lag represent one read, one read every 11 seconds. C) present the slice form data plot in A), respective situation with D) and B). On A),C) and B),D) there are results of different potential channels measured in different plants in the same experiment. On E) and F) channels 1 & 2 respectively, 1,000 reads from another experiment on tobacco. No clear trends or seasonality related to the operating light color or time of day was found.

reads from different light groups seems useful in order to remove seasonality and to find structure in the data (using the above mentioned software library: pandas.diff(); periods of 110; 220; 330; 440). The time periods investigated with the Diff()-method were directly related to length of one light wavelength phase, that is, 20 min and multiples. This method did not help in finding any hidden data structure and seasonality (see Fig. 11).

In order to use machine learning classification methods, the datasets were fragmented according to the light color operating on plants, that is, 110 reads per fragment labeled with the respective light color for each. Random forest and k-Nearest-Neighbours (KNN) were used as classification methods on statistical values of datasets for every light cycle. Statistical values were used as the light cycle's features were: min(), max(), mean(), median(), and kurtosis(). Different parameters were tested: k for KNN in range 1 to $n-1$, n-estimators in a range of 1 to 100 for random forests. The training set and the test set were 70% and 30% of the full dataset (from 12,000 to over 100,000 reads). Accuracy for both methods was lower than or similar to random classification probability. So we found that light-labeled data does not differ, if we consider statistical parameters. The same machine learning methods run on raw electric potential data also do not find any efficient light color classifications. None of the tested machine learning methods allowed for efficient classification of light cycles corresponding to different light color

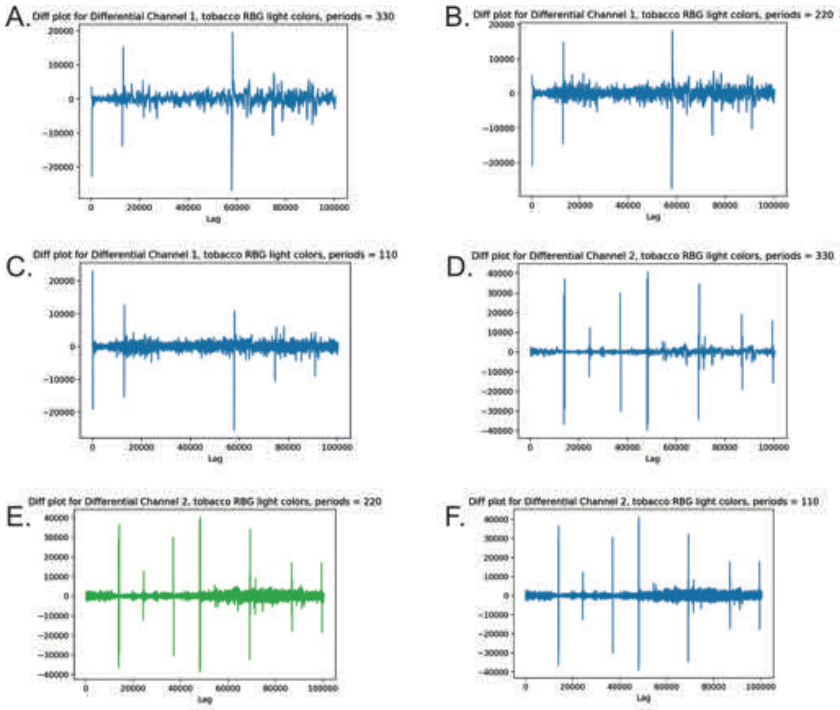

Figure 11: Example plots of plants electric potentials from Phytosensor measurements after applying difference method to Phytosensor data. Periods of 330, 220, and 110 are the length of one light color phase, that is, 20¿min. One lag represent one read, one read every 11¿seconds; A), B), C) show the same channel with applied different number of periods to calculate diff(). Respectively D), E), F) the second channel form the same experiment. No clear trends or seasonality related to operating light color were found after using difference methods.

classes. Given the current state of development of the Phytosensor, the obtained data doesn't allow for direct light color detection from data 'processed' in plant stem.

The data was found to be (at least for some of the datasets) mostly free of time correlations but for some time series we found time-dependent characteristics. We did not find any dependency on light wavelengths. Augmented Dickey-Fuller Tests (ADF) and autocorrelation plots inspections were done to evaluate if the time series are time-dependent, see Fig. 13. However, for most of the experiments the Augmented Dickey-Fuller Test (ADF) suggested that data was not time dependent. Different statistical models were applied to plant electric potential data: autoregression model, Autoregressive Integrated Moving Average (ARIMA(p, d, q)), Seasonal AutoRegressive Integrated Moving Average with eXogenous regressors model (SARIMAX), and Holt-Winters exponential smoothing, see Figs. 12 and 14. None of these models has predictive power. However, a closer look on some dataset fragments revealed some repetitive patterns in the potential changes. These do not simply overlap with light phases, but may be light-dependent in more complex ways. Without correlation with time it is feasible to start working with the ARIMA model as means do not differ within dataset fragments. Although we used an extensive grid search for optimal ARIMA parameters, the forecasting power of the model was still rather poor. The predictions were all ill-formed and predicted trivial patterns for the whole dataset.

Interestingly, correlations between two differential potential channels differ a lot between

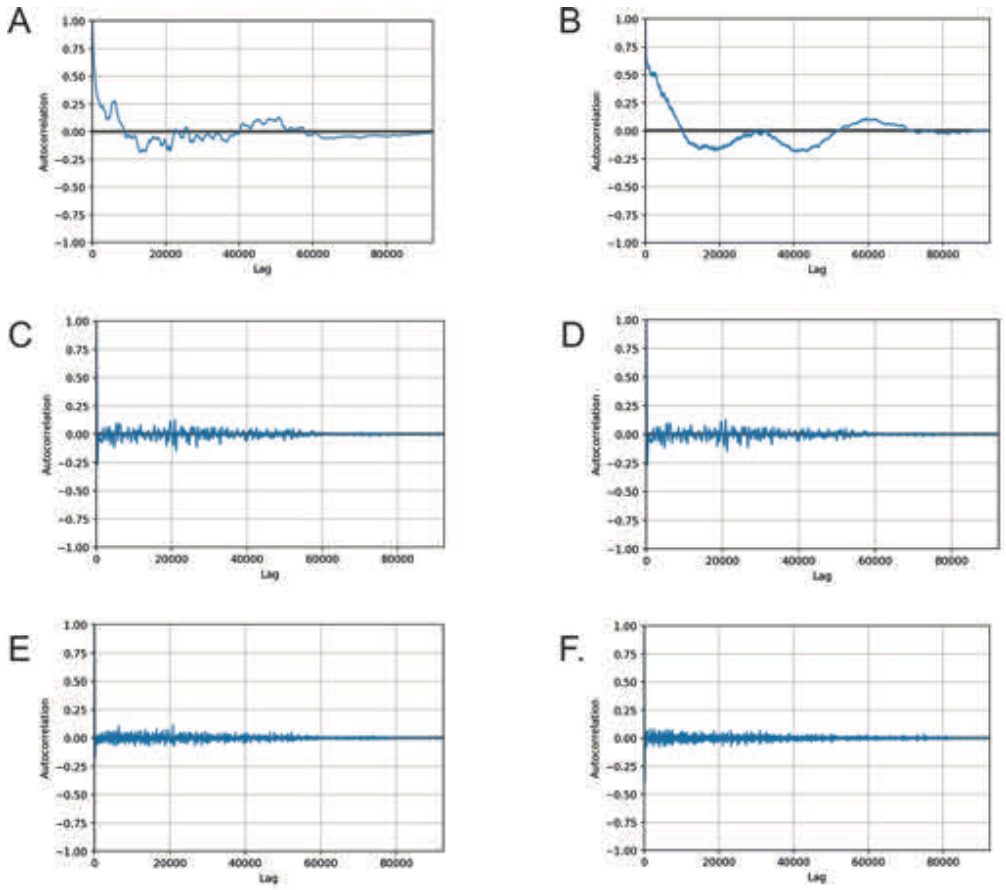

Figure 12: Autoregression prediction results for both channels from three experiments with tobacco A-D and tomato E-F; red line: autoregression results; blue line: test data.

different measurements, despite their similar experimental designs. For most of the dataset correlations between differential potential channels was below 0.2. This was rather surprising because the needles for both channels were inserted into plants, that were growing in the same conditions, and the electrodes were inserted into analogous organ points. Therefore, the strong correlations between channels were expected. The lack of these correlations may indicate strong individual variance between datasets caused by the influence of microscopic differences in insertions of electrodes. Different types of tissue could be reached and different damages could occur within plants organs.

The extensive analysis of plant-electrophysiological data was done in order to elucidate changes in plants electric potentials in response to different light wavelengths. In future work, we plan to test artificial neural nets (e.g., LSTMs) for the recognition of patterns in the electrophysiological data. Applying LSTMs may prove to be helpful in order to find a characteristic response to changing light wavelengths or responses to other temporal patterns in electric potentials. Considering a longer time horizon and research perspective, also other experimental setups would be worth to consider, such as using other light sources or inserting electrodes in other plant organs or in different ways. One of the main reasons of the slow progress in deciphering plant's electrical signals is the lack of efficient methods to measure electrical potentials in the

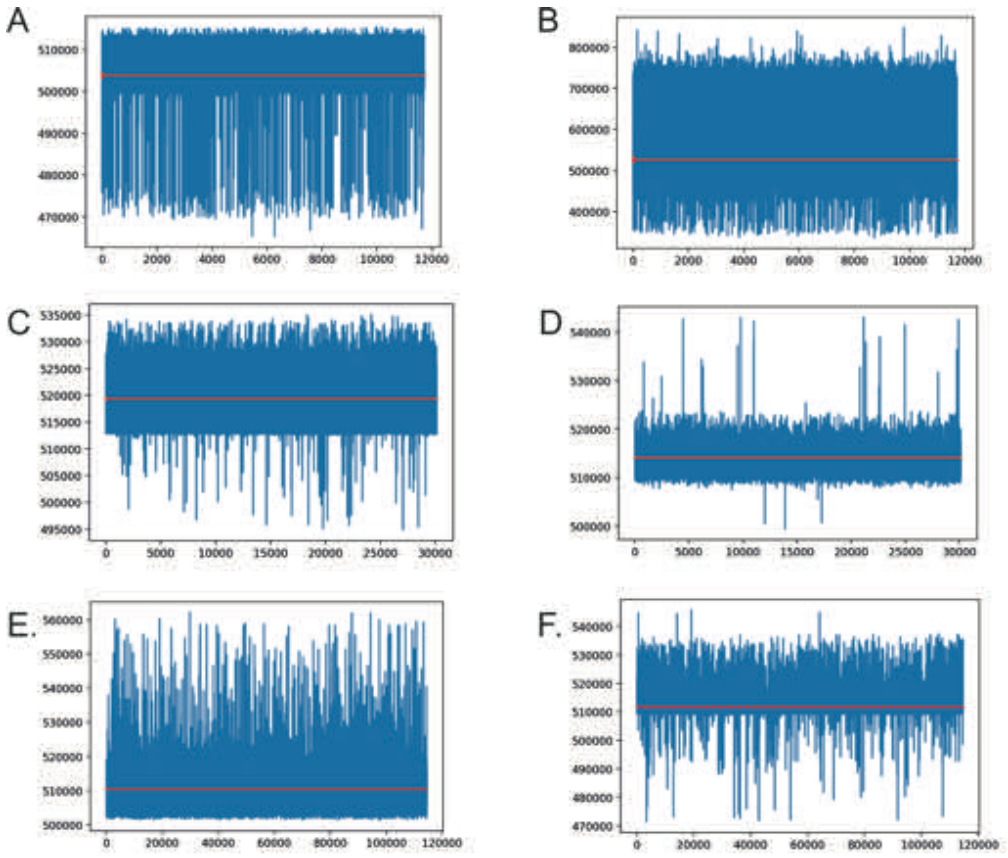

Figure 13: A, B: Autocorrelation plots from two channels; C), D: autocorrelation difference (periods = 110) plots from respectively data plotted on A and B; E, F: autocorrelation difference (periods = 330) plots from respectively data plotted on A and B.

tissue/cells of interest. The differences of detected plant reactions to switched on light here and in the next section might be caused by different experiment setups on the level of insertion of electrodes, subjected plant species, and their anatomy. Moreover, updating the hardware and the light color in the Phytosensor readings may ensure that light labels will be added to the correct sensor readings.

A plant damage detection, assuming that no other stress occurs, is presented in the following. Moreover, first successful applications of plant electric biopotentials in simple bio-hybrid systems are also described. Changes in potentials after switching light on/off are detected. We also find that using the Phytosensor to detect whether light reaches a plant, may be feasible in the future.

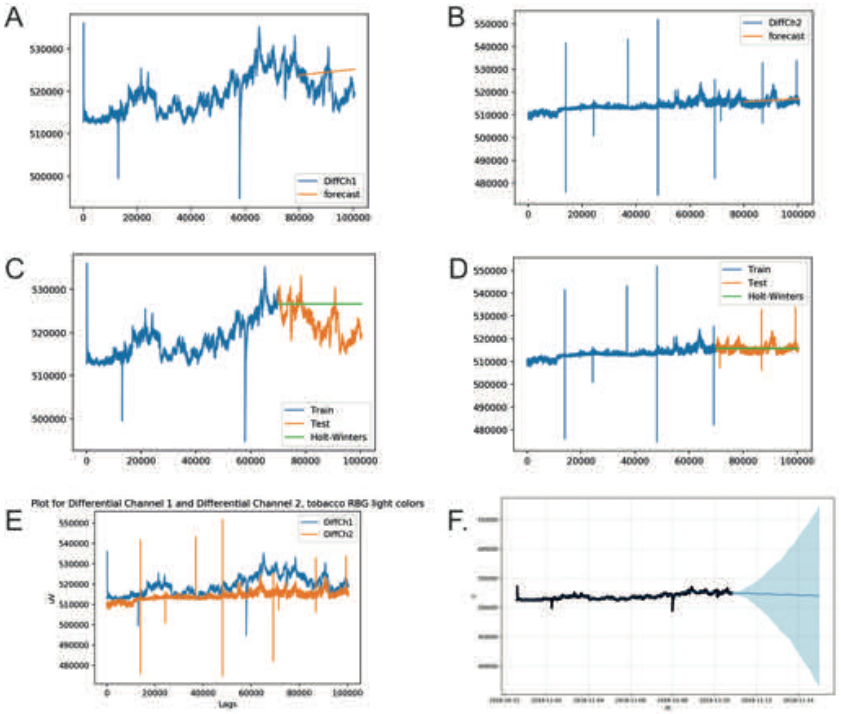

Figure 14: A, B: Results of ARIMA model prediction for two channels from the same experiment; C, D: results of Holt-Winters model prediction for two channels from the same experiment; E: both channels plotted together; F: results of forecast done with fbprophet. Channel 1 is also presented on A and C and is one of the rare dataset with more complex data structure.

4.2 Application of Phytosensor in plants damage detection

In our bio-hybrid experiments we plan to use Phytosensor bio-potential measurements to detect damages of plants, such as cutting leaves or branches. The idea is to detect short-time plant reactions for different types of stimulation, such as light, touching leaves, temperature changes, etc. These cannot always be clearly distinguished, however, we assume that cutting leaves is a strong stimulation simplifying the task slightly. We would need to find clearly distinctive spikes compared to the background signal of bio-potentials.

In Fig. 15 we show the results of our experiment for detecting cut leaves by bio-potential measurements. The reactions of two similar Dracaena plants were measured with two Phytosensors. The two channels of bio-potential measurements were used at each Phytosensor, that were connected at different branches of the same plant. The reaction of channels 1 and 2 in plants A and B are different. We call them: high-spike and low-spike. Plant B generates high-spikes and low-spikes. Plant A generates two low-spikes. The actual form of the spikes depends on the placement of the electrodes and on the polarity of the electrodes. It may even be possible not only to detect a damaged plant but also to localize the cut within a plant's architecture.

The signal of the cut plant was characterized by different circadian bio-potential values and it reacted dissimilar to a stimulation compared to the undamaged plant. In Fig. 16 we show data of two weeks of a bio-potential signal from a branch that was not cut (red line) and a branch that was cut (black line). By cutting a branch, the plant's integrity was interrupted and also its vascular tissues. We observed that withering of the cut branch did not limit the detection of the bio-potential circadian cycle that is similar to the healthy, uncut branch. Measured potential signals are specific for living plant tissues and disappear quickly with cell death. As a next step, the identified 'cut-specific' spikes should be compared with spikes triggered by other stresses to verify their uniqueness.

4.3 Coupling of Phyto-sensing with light stimulation

The use of the Phytosensor is not limited to measuring plant reactions to stresses, it can also be used for the actuation and stimulation of plants (see Fig. 17). The actuator added to system does not only measure the plant potentials, but also influences the plant. Hence, we close the feedback loop in our bio-hybrid system.

In this experimental setup, we combine the Phytosensor with electrodes inserted into a Ficus and an additional sensor stick for environmental monitoring (see Fig. 18). Two different actuators (plant stimulus) were added to the system to trigger plant reactions: a red/blue plant growth LED lamp (28 W) and and room fan (25 W). The experiment partially follows the work of Gagliano et al. [3]. The actuators were connected to the PC-controlled power outlet relay module. Hence, we establish a possibility to switch on/off the LED lamp and the fan by software. Our key assumptions for this experiment are:

- We consider the 'external observable parameter' as the output measure (e.g., light is a part of the bio-hybrid system, on/off time as an output parameter).
- The feedback loop changes the observable output parameter.
- The environmental stimuli affect the system, thus we can observe a complex plant response.

In Fig. 19 we give a schematic overview of the experiment with imposed feedback loop based on bio-potential measurements. The LED lamp was turned on and off by the processed bio-potential Channel 1 signal (Z-score calculations, see Fig. 19). The Z-score (standard score) value of the bio-potential is calculated by a moving window average and compare to a predefined

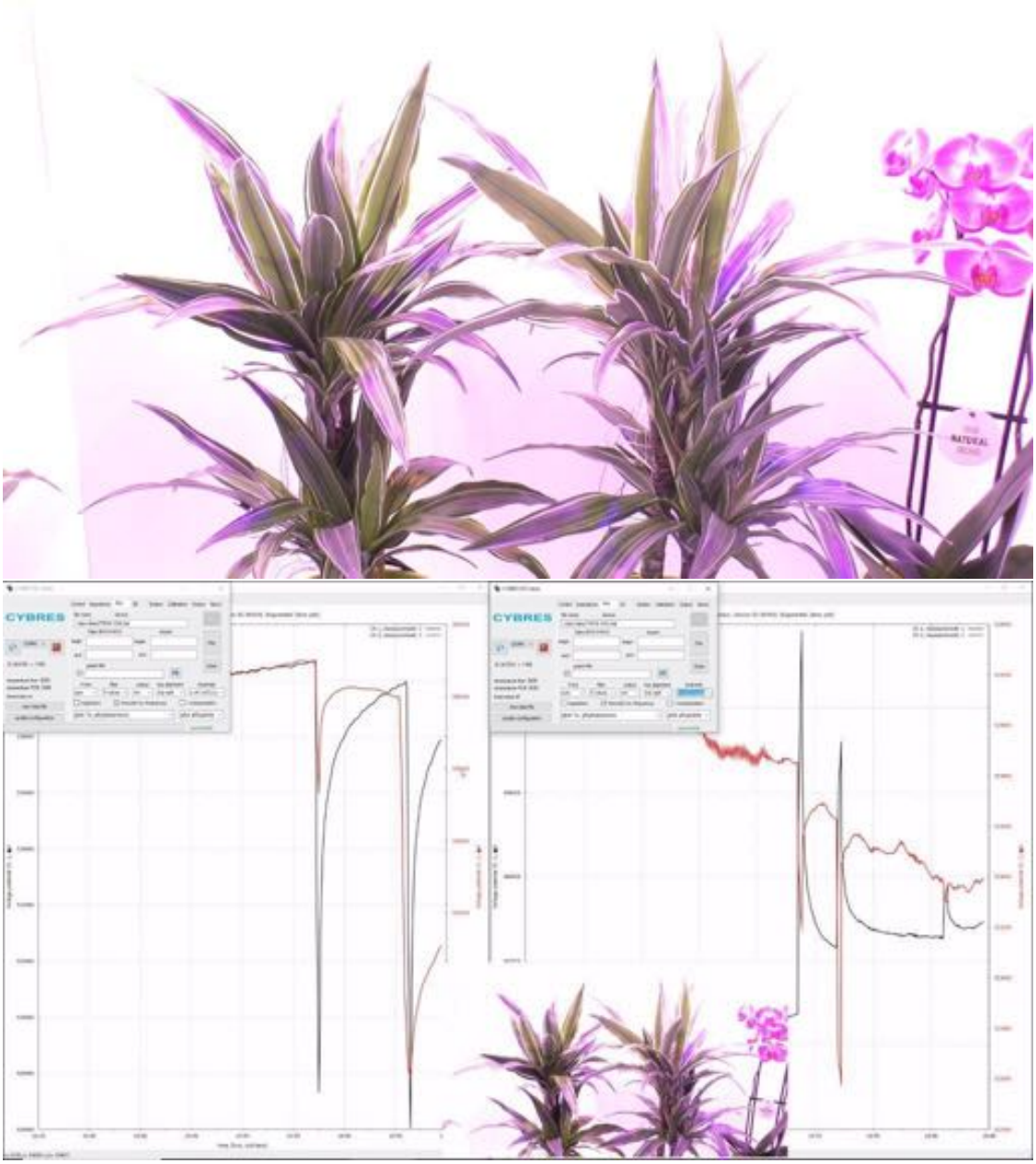

Figure 15: Detection of the plant damage (cutting leaves) with 'spiking' reaction at bio-potential measurement. Two Dracaena plants were cut and their potentials were measured: left: plant A; right: plant B.

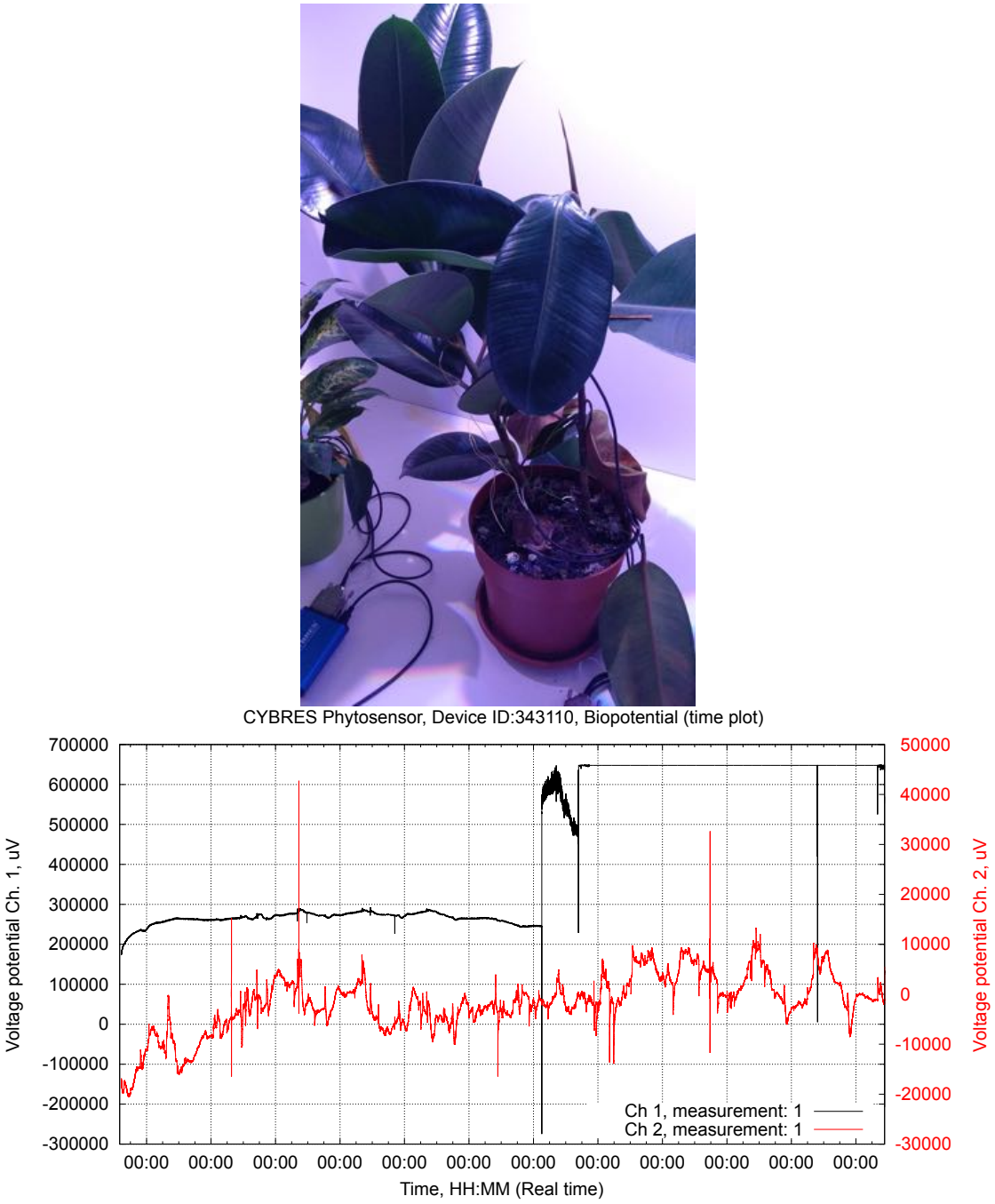

Figure 16: Detecting a cut branch: bio-potential measurement showing long-term circadian cycle and different behaviors between the undamaged (**red line**) and damaged (**black line**) branch of the Ficus plant.

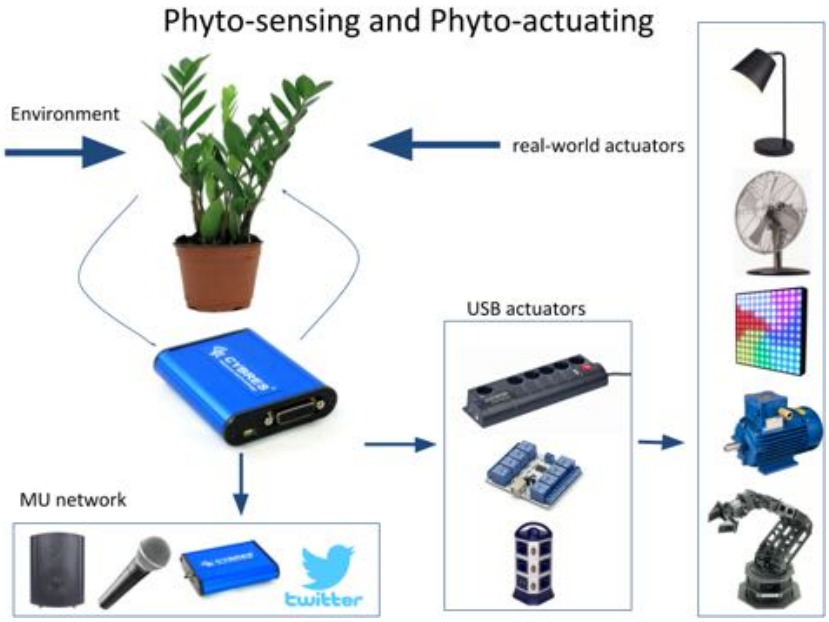

Figure 17: The extension of Phytosensing system that will provide the phyto-actuating and interaction with users.

constant threshold. In the case that the Z-score is greater than the threshold we turn the light on, otherwise we turn it off. The logic is the following: an increase of 'Z-based noise' in the bio-potential signal of Channel 1 during the 'light OFF-phase is necessary to turn the light on.

We ran the experiment for a few days and interesting plant responses were discovered (see Fig. 20). The bio-potentials within the Z-based feedback loop after a few days of 'training' lead to turning off the light (the point 'A', evening) and turning on the light (the point 'B', morning) autonomously (see Fig. 20c). This can be interpreted as an indicator for adaptive physiological functionality.

After a few days of Z-based light control, the light on/off phases were set to periodical control with a 10 minutes 'light on' phase and a 10 minutes 'light off' phase. During the initial hours of the experiment, an excessive noise level (Channel 1) in the 'light off' state was observed (see Fig. 21, a, black line). Note that in previous experiments with the same plant and setup the increase of Z-based noise in the bio-potential signal of Channel 1 during the 'light off' phase was the condition to trigger the 'light on' event. An interesting observation was made after ∼8 hours of periodical light on/off control. Channel 1 was not perturbed with excessive noise anymore and then the electric potential of plant seemed different (see Fig. 21b, black line). The continuation of this bio-potential measurement experiment with periodic light on/off control is shown in Fig. 22.

The periodic 10 min light on/off plant excitation lasted for two days. At one moment we deactivated the periodic light on/off control script, that is, there was no further light excitation. During the next expected 'light on' event (the event did not occur as the light was turned off) the bio-potential almost exactly reacted in the same way as previously, but without external light stimulus (see Fig. 23, red point A). This experiment suggests that plants have an ability to adapt to cyclic excitations.

In the next experiment, we introduce the second stimulus. Along with light we use a fan as neutral stimulus. The periodic 10 min on/off phases were used as before, but now we split the

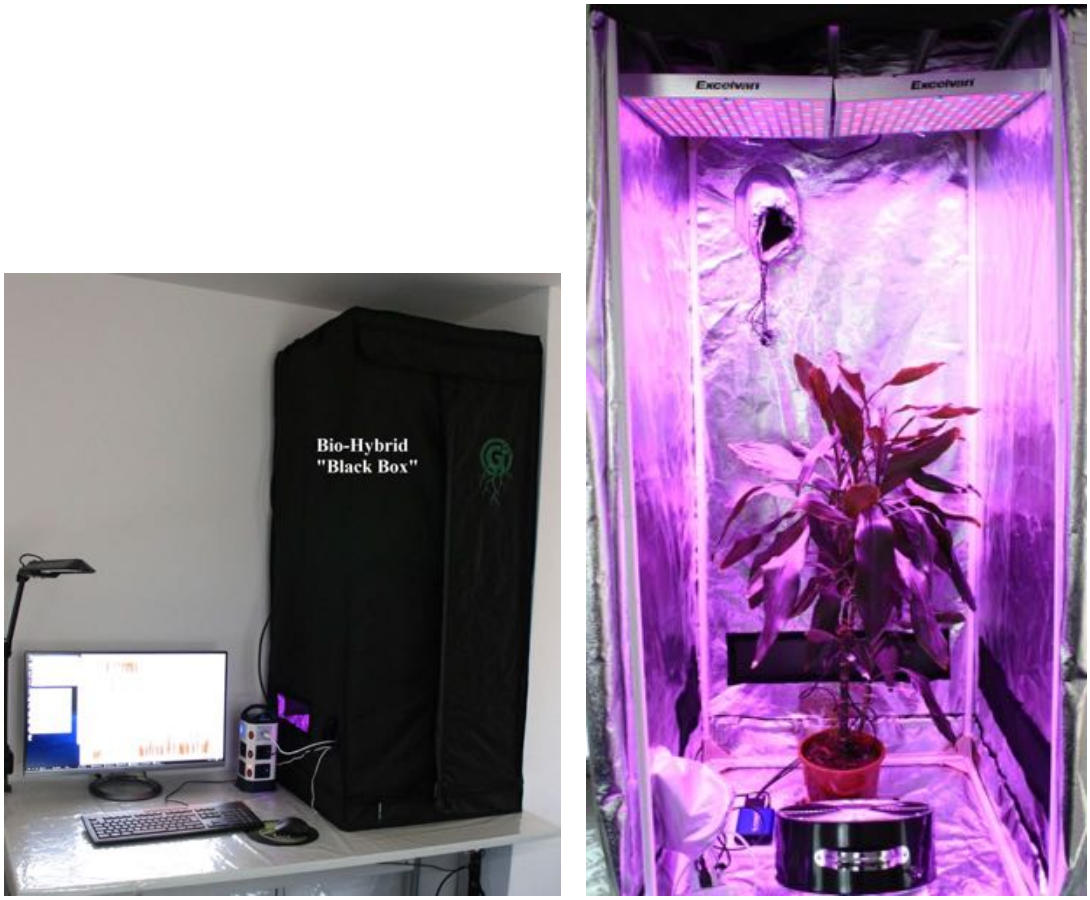

Figure 18: The plant bio-hybrid 'black-box' experimental setup. Ficus plants with two differential potentials channels measured by Phytosensor. The light which was switching ON/OFF was the only light source for the 'in-black box' plant.

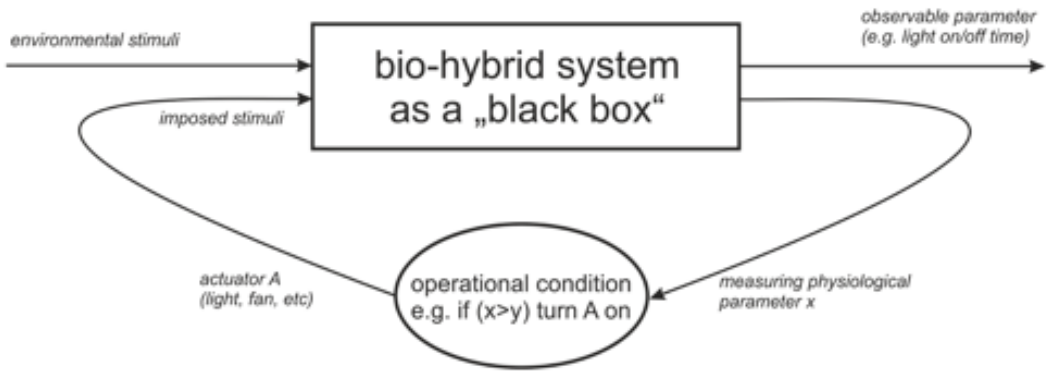

(a)

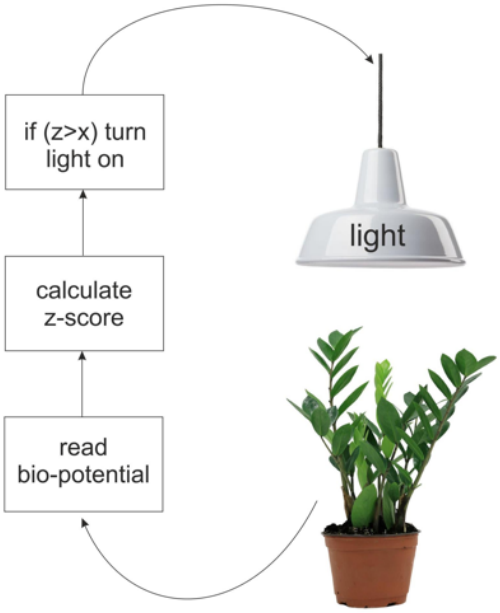

(b)

Figure 19: (a) The plant bio-hybrid system as 'black-box'; (b) schematics of reinforced training within the bio-potential z-based feedback loop.

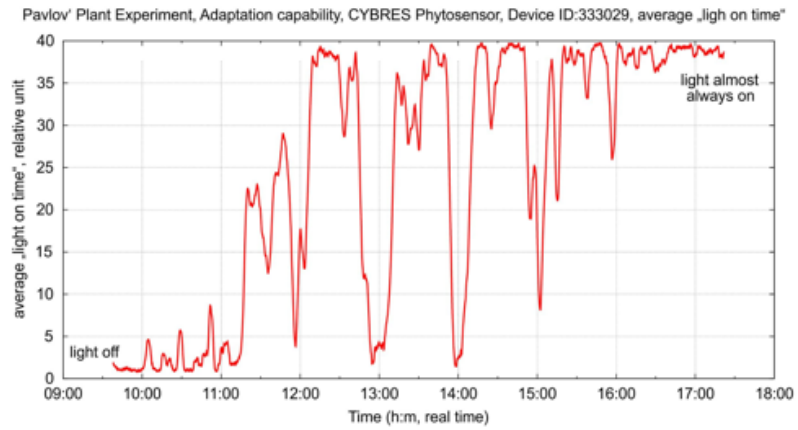

(a)

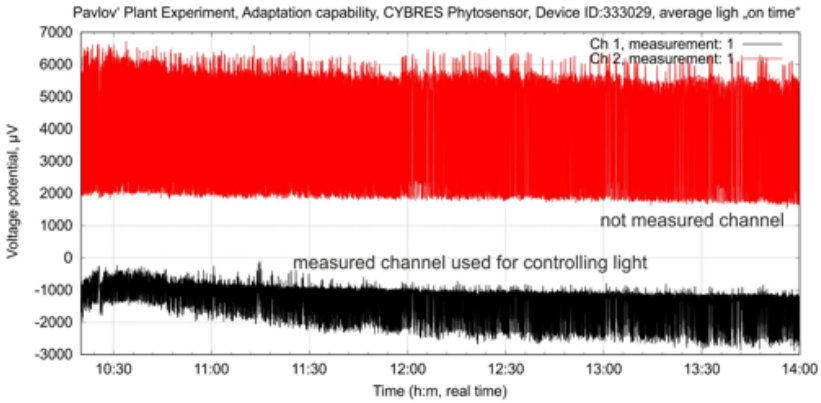

(b)

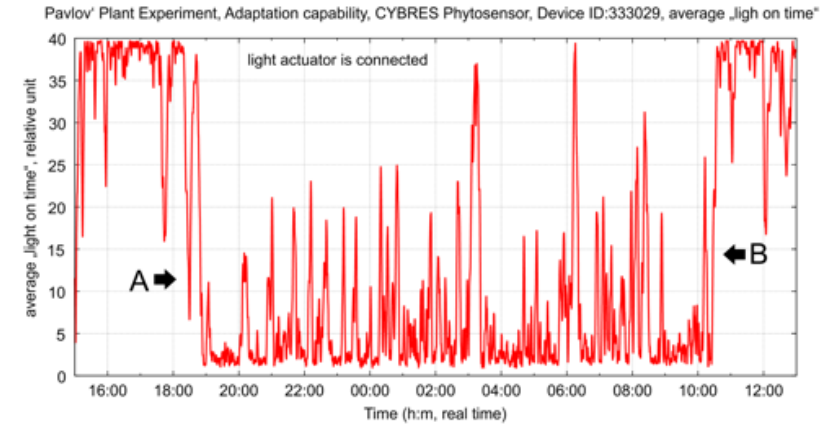

(c)

Figure 20: a) Screenshot of 'light on' events; b) potentials measured in different branches; c) plant 'self-regulation' of illumination time.

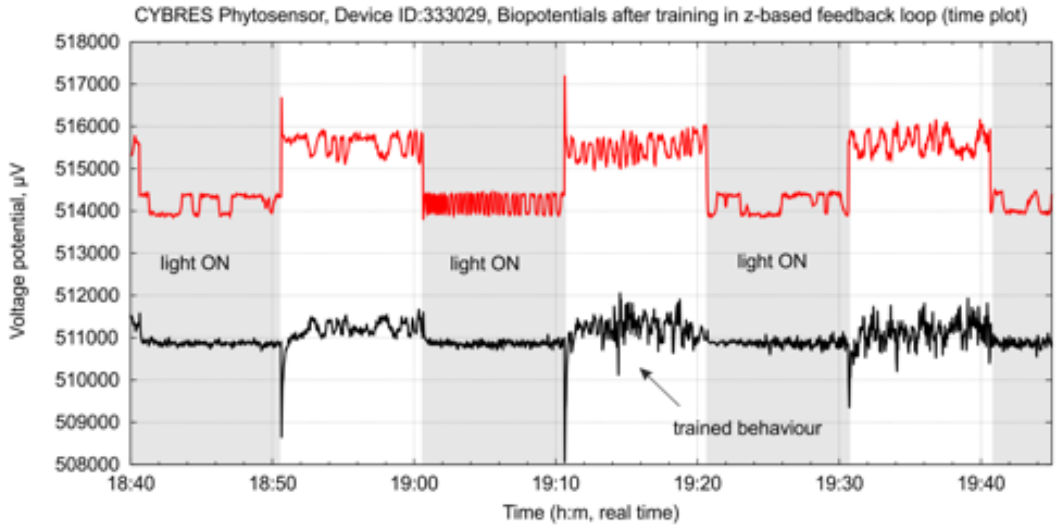

(a)

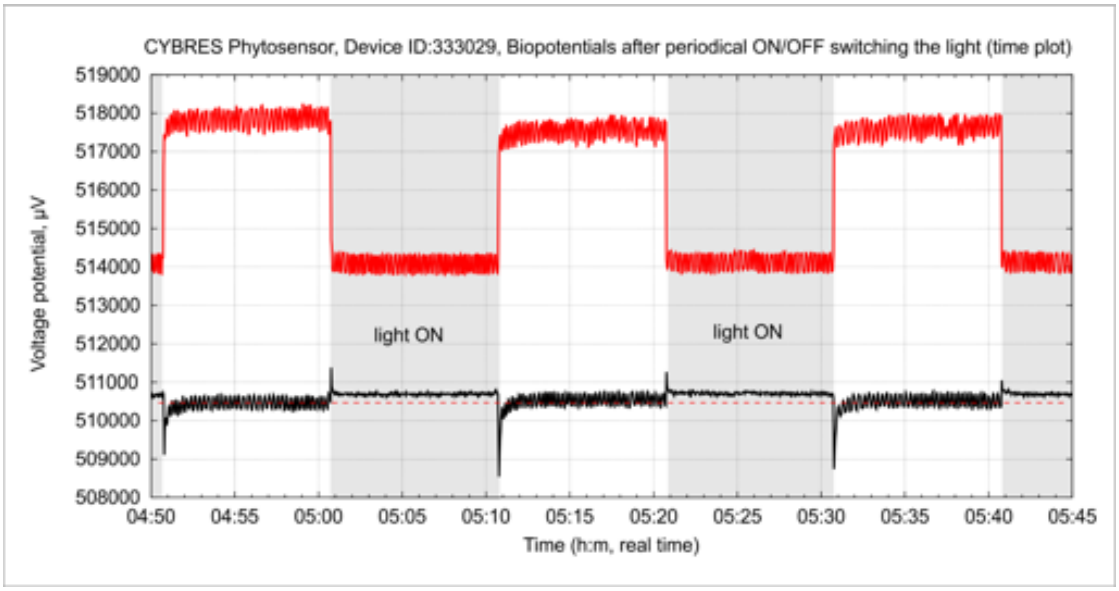

(b)

Figure 21: Bio-potentials in two channels for Dracaena plant, periodic 'light on' and 'light off' control. (a) z-based feedback loop light control; (b) ∼8 hours after z-based feedback loop light control.

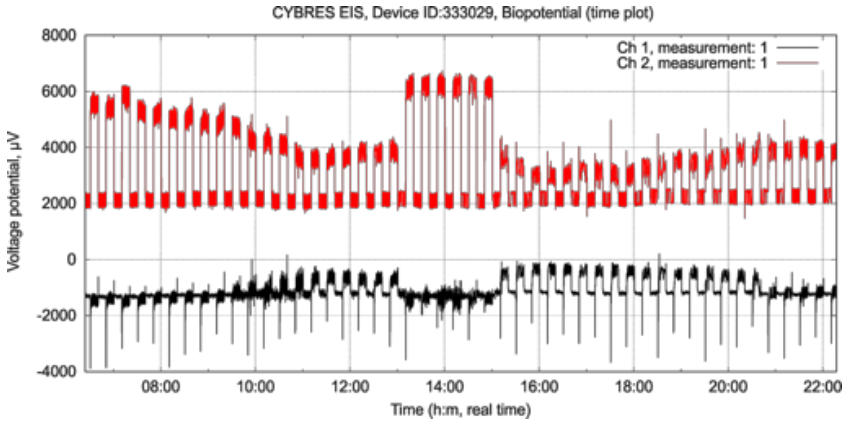

(a)

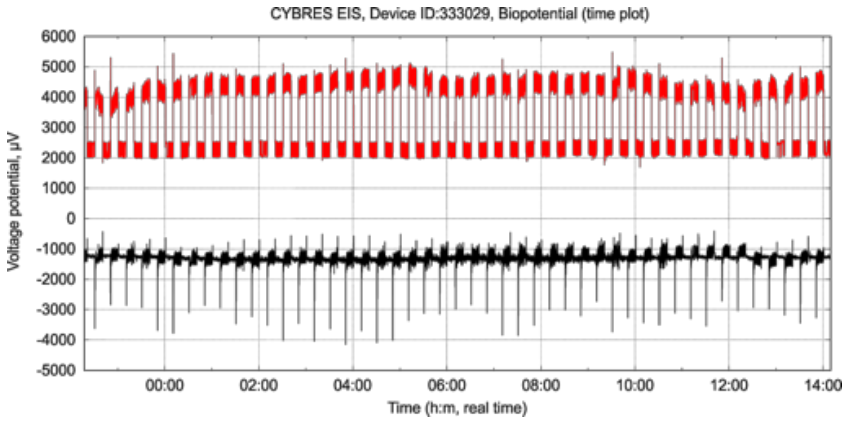

(b)

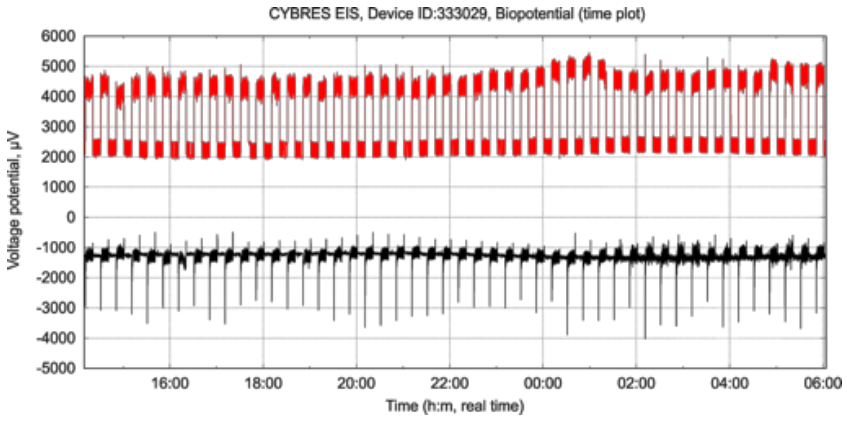

(c)

Figure 22: Bio-potentials in two channels for Dracaena plant, periodic 'light on' and 'light off' control. (a) ∼8 hours later; (b) ∼24 hours later; (c) ∼48 hours later.

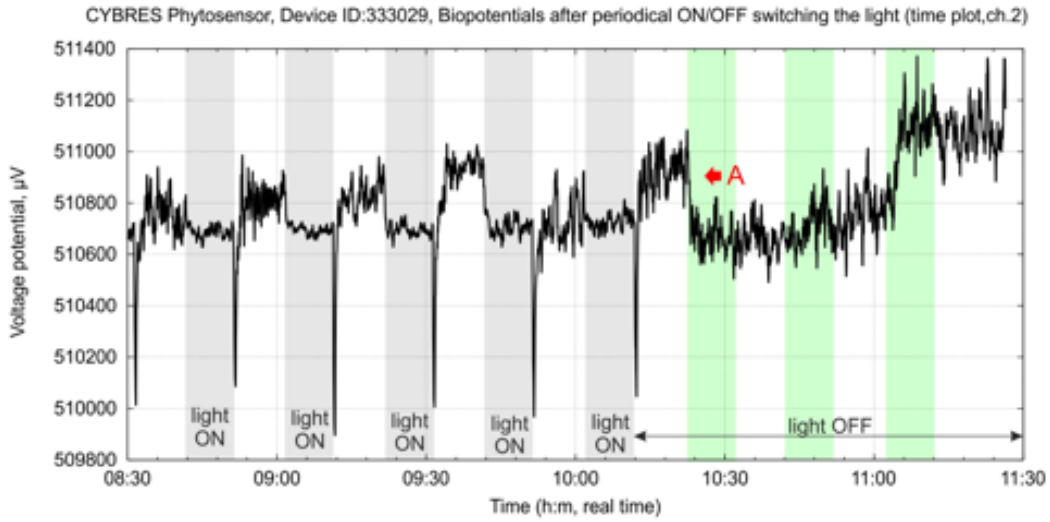

Figure 23: The Dracaena plant bio-potentials after periodic light on/off control algorithm was terminated and light was constantly off.

experiment into three training phases:

1. Only the fan is operating; periodic 10 min on/off cycles; duration of 6 hours.
2. The light and the fan are operating; periodic 10 min on/off cycles; duration of 12 hours.
3. The fan is operating only; periodic 10 min on/off cycles; duration of3 hours.

The results of this experiment are shown in Fig. 24. We summarize:

1. No spikes in the bio-potential signal at the moment of the 'stimulus off' event in this phase (only fan is operating).
2. There are spikes in the bio-potential signal at the moment of the 'stimulus off' event in this phase (fan & light are operating). We assume that the periodic light on/off excitation triggered these spikes.
3. There are spikes in the bio-potential signal at the moment of 'stimulus off' event in this phase (only fan is operating). The spikes last for the first two to three hours and no spikes are observed when only the fan operates in the on/off excitation experiment again.

Associative learning in plants was reported by Gagliano et al. [3] and could be implemented in *flora robotica* using the Phytosensor. In the future this may result in development of innovative and more efficient bio-hybrid technologies.

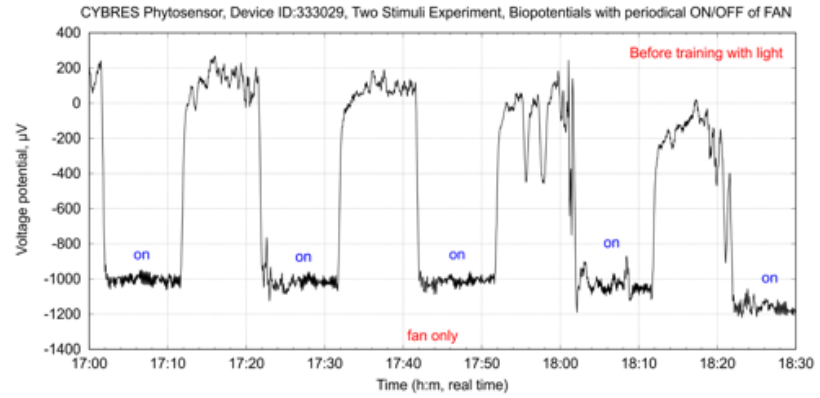

(a)

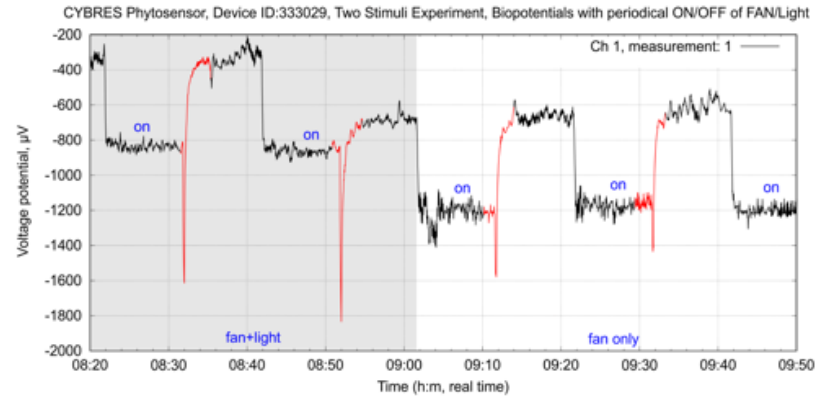

(b)

Figure 24: The Dracaena plant bio-potentials with periodic excitation training using two stimuli (fan and light); (a) training phase 1, only fan is operating; (b) training phase 2, fan & light are operating, and training phase 3, only the fan is operating.

5 Vascular Morphogenesis Controller (VMC): further investigations of morphological behaviors

The Vascular Morphogenesis Controller (VMC) is a distributed model of morphogenesis inspired by the competitions between branches of plants for common resources. The model has been initially introduced in D2.2 and has been improved and investigated for effects of certain parameters in D2.3. Here we continue our study in terms of morphological and dynamic behaviors in a set of simulations. The physical implementation of the model studied in a series of scenarios in guiding the growth of braided structures is presented in D3.3.

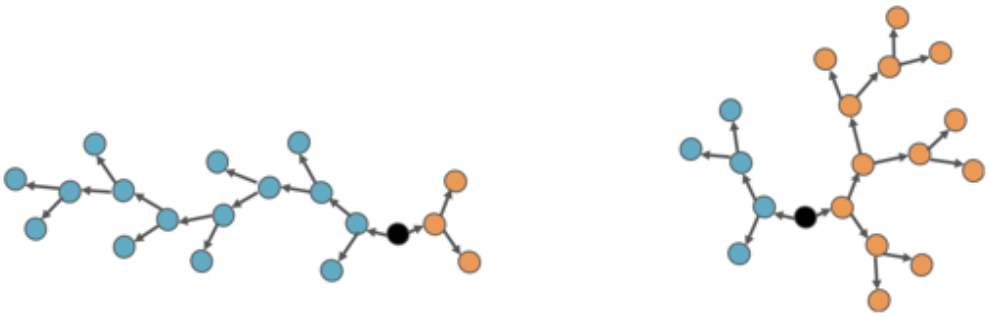

Figure 25: A schematic of two example structures with the same number of nodes. The nodes at the left main branch are indicated in blue and the nodes at the right main branch are indicated in orange.

In D2.3, we have studied a number of morphological features of a particular implementation of VMC. Here we use a similar framework of simulations but we switch to a stochastic implementation of growth in respect to the addition and deletion of nodes and look more closely into a selected number of intrinsic morphological and dynamic behaviors of VMC.

The study is performed for the internal tendency of the VMC structures towards asymmetry of the shape and dynamics of the morphology (i.e., growth and retraction) in the absence of any environmental asymmetry (e.g., any variation or gradient existing in the environment) or structural information. For that, no external effects including sensory information and physical interactions between the different parts of the structure or between the structure and environment are implemented. Therefore, the dynamics and behaviors are merely the result of internal interactions and dynamics via the vessel system. We limit the study to a setup with one root node and two children for every node. The simulation starts with the root node and its two children: one child positioned at the left side and the other at the right side of the root. None of the nodes of this initial structure are allowed to be removed during the experiment. Fig. 25 shows two schematic example structures with the same number of nodes and different shapes. In the following, the set of experiments investigating some of the intrinsic morphological behaviors of the VMC due to different parameterizations are presented. Since there is no environmental information, all the sensor-dependent parameters are set to zero in all the experiments.

5.1 Morphological Aspects: Asymmetry and Adaptivity

The two children of the root start the two main branches of the structure. The asymmetry of the grown structures in respect to these two main branches is measured. The asymmetry is defined

here as the absolute difference between the proportion of nodes at the two main branches at the end of a run

$$\text{asymmetry} = \frac{|N_{\text{L}} - N_{\text{R}}|}{N_{\text{total}}}\,, \tag{1}$$

where N_{L} and N_{R} are the number of nodes at the left and right side of the structure respectively, and N_{total} represents the structure's size which is the total number of nodes excluding the root.

In addition to asymmetry regarding the final morphology of the structure, we define a measure of dynamicity capturing an aspect of changes in the structure during the growth process. Dynamicity is defined as the proportion of deleted nodes during the growth process of the structure to the final size of the structure

$$\text{dynamicity} = \frac{D}{N_{\text{total}}}\,, \tag{2}$$

where D is the number of nodes that are deleted during the course of the experiment.

A set of simulation runs with different parameterizations are performed. Every run starts with the root node and its immediate children and grows for a period of time. To define a stop condition for a run, the maximum size of the structure during development is recorded and the run continues until 50 time steps after the recorded maximum size. Reaching this stop condition in a limited time period is guaranteed by setting the consumption rate of the nodes (c) to a positive value that constrains the size of the structure. Since all the sensor-dependent parameters are set to zero, in the following we respectively use β, ρ, and ω to indicate β_{c}, ρ_{c}, and ω_{c}. Note that without the sensory information, the successin produced in all the leaves are the equal.

Table 1: List of parameters and their values

parameter	value
α	$0.1, 0.5, 0.9$
β	$0, 0.5, 1.0, 2.0, 10.0$
ρ	$0.25, 0.5, 0.8, 1.0$
ω	$0, 0.1, 1.0$
c	1
R_{root}	20

Table 1 shows the different parameter values used in the simulations. Every parameterization is executed for 25 independent repetitions. In this implementation, children of a node are deleted with a high probability (95%) if all of them have a resource value below 1 ($th_{del} = 1$). Probability of adding children to a leaf i is proportional to the share of resource at the leaf (R_i/R_{root}). Perfectly simultaneous growth of different leaves is avoided by randomly choosing one leaf at a time step from the pool of candidate leaves.

Fig. 26 shows the *asymmetry*, and *dynamicity* of the different setups and the size of the structures in each case. The bars represent the values averaged over all repetitions and the whiskers represent the standard deviations. As seen in the figure, $\omega = 0$ leads to relatively symmetric structures with a medium number of nodes and low dynamicity. This is due to the fact that without any input (sensor) value or constant production rate, no successin is produced and therefore there is no difference between the thickness of vessels leading to equal distribution of resource independent of other parameters. The minimal asymmetry is only due to the transient effect of random choice of leaves for growth.

For the setups with $\beta \leq 1$, the structures are symmetric. This is inline with results of our theoretical analysis in D2.3 implying that $\beta \leq 1$ is a sufficient (but not necessary) condition for tendency towards growing symmetrically, when all other things are equal.

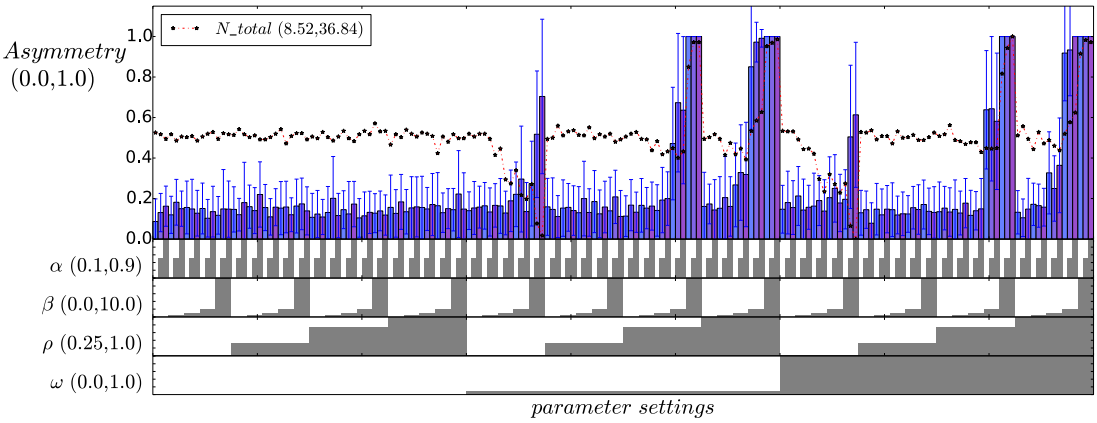

(a)

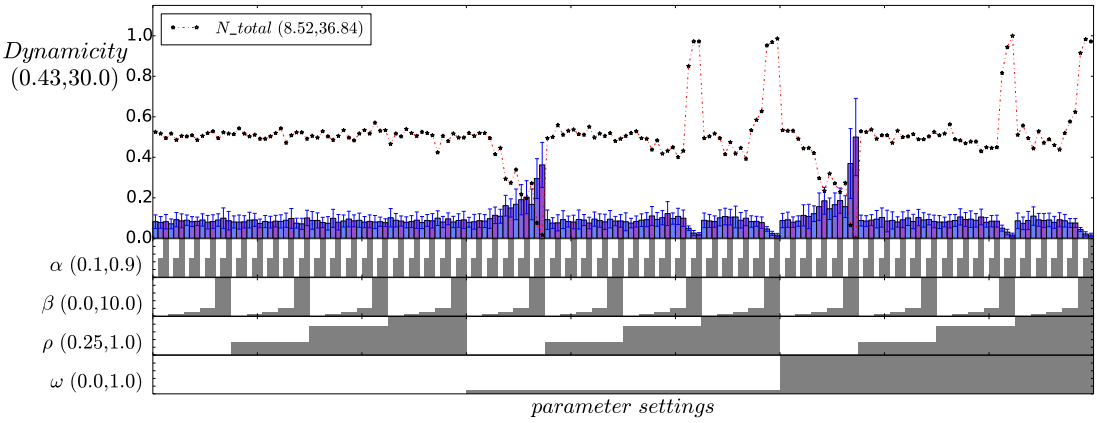

(b)

Figure 26: Asymmetry and dynamicity of VMC structures with different parameterizations. The colored bars (top part) represent the values averaged over all the repetitions and the whiskers represent the standard deviations. The red dots represent the number of nodes in the structure at the end of the runs. The gray bars (bottom part) indicate the values of each parameter.

For values of $\omega > 0$, $\rho > 0.5$, $\beta > 1$, the structures are asymmetric with low dynamicity. With the high value of $\beta = 10$, dynamicity is minimal, reflecting the low amount of deletion occurring during growth.

For values of $\rho \leq 0.5 = \frac{1}{n}$ (where $n = 2$ is the number of children of a node), the structures are symmetric except for the setup with $\omega > 0$, $\rho = 0.25$, $\beta = 10$. This exception seems to be deviating from the theoretical analysis[1] presented in D2.3 which stated that the necessary condition for a tendency towards asymmetry is $\rho > \frac{1}{n}$ and therefore predicting symmetry for $\rho < \frac{1}{n}$. The same effect (high asymmetry and deviation from the theory) can be also seen for other values of $\rho < \frac{1}{n}$ (an example will be shown below). The reason for this unpredicted behavior is the delay in the updating of the values within the structure. It is more clear when looking at the extreme case of $\rho = 0$. In this case, no successin passes from one level to the next.

[1]Note that the analysis assumed convergence of values which is not necessarily the case for all setups

Therefore, the only effect of successin is to regulate the thickness of the immediate connections of the leaves and other connections always get a successin of zero. Consider the process of growth starting from the initial structure (the root and its two children). In the beginning, both leaves get the same amount of resource and have equal chances to grow. After the first growth event (at either branch), the weight of the connection behind the grown node starts to decay towards zero (with rate α) because it is not an immediate connection of a leaf and thus gets no successin. Therefore, the branch gets a decreasing share of the resource. However, the resource that was already delivered to that node continues its distribution among the child nodes. Every leaf with a large share of resource is likely to grow. This applies also to new leaves as they emerge. For some time, the grown branch has higher chances for growth due to larger number of leaves that still hold enough resource to grow. Eventually, the resource is too much divided at the side of the grown branch and the chances for further growth decrease. Meanwhile, the resource at the single leaf of the other side has increased due to the presence of successin at its immediate connection to the root versus no successin at the other side (no immediate leaf). Therefore, the short side starts growing with a large amount of resource which again goes through the same process of decay of connections and division of resource. In parallel to this new growth, the previously larger side loses its nodes due to their small resource values until there are no nodes left except the initial leaf of that side. The leaf has now an immediate connection to the root again and attracts the resource. Thus the fluctuating asymmetry between the two main branches continues. The fluctuation can be recognized by looking at the measure of dynamicity and the size of the structure. In Fig. 26(b), comparatively high values of dynamicity and low number of nodes (small size of structure) are observed for all setups with $\omega > 0$, $\rho = 0.25$, $\beta > 1$. Recall that the dynamicity reflects the proportion of deletion rate during the growth process relative to the size of the structures.

Fig. 27 shows the asymmetry and dynamicity along with the number of nodes for a parameter sweep experiment on the values of ρ in a setup with $\omega = 0.1$, $\beta = 10$, and $\alpha = 0.9$. As seen in the figure, around the critical value of $\rho = 0.5 = \frac{1}{n}$ (where $n = 2$ is the number of children of a node), the behavior changes from high dynamicity and small structures (small number of nodes) to large and stable structures. The measured asymmetry increases both above and below the critical value. Above the value, the increase in asymmetry (up to fully asymmetric structures for larger values of ρ) is accompanied by an increase in the number of nodes and a decrease in dynamicity. That means, if the $\rho > \frac{1}{n}$, large stable structures grow increasingly asymmetric for the higher values of ρ. Below the critical value ($\rho < \frac{1}{n}$), the high asymmetry along with the very small number of nodes and high dynamicity indicates fluctuations of small unstable structures with a few nodes repeatedly growing and disappearing again in one side or the other.

Another example of parameter sweep experiment on the values of ρ is shown Fig. 28. The figure demonstrates asymmetry, dynamicity and the number of nodes for the setups with $\omega = 0.1$, $\beta = 2$, and $\alpha = 0.9$. Around the critical value of $\rho = 0.5 = \frac{1}{n}$ (where $n = 2$ is the number of children of a node), the behavior changes from high dynamicity and small fluctuating structures to large and stable structures.

5.2 Decision Making Performance of the Collective System

Due to the probabilistic nature of the current implementation for addition and deletion events, every growth trajectory shows a number of fluctuations in the number of nodes at each side of the structure. Likewise, the amount of resources assigned to each side changes. Fig. 29 shows a set of example dynamics of r_L, the fraction of resource assigned to the left side of the structure, which is calculated as $r_L = R_L/(R_L + R_R)$.

As expected from the previous section, the behaviors for the various settings demonstrated

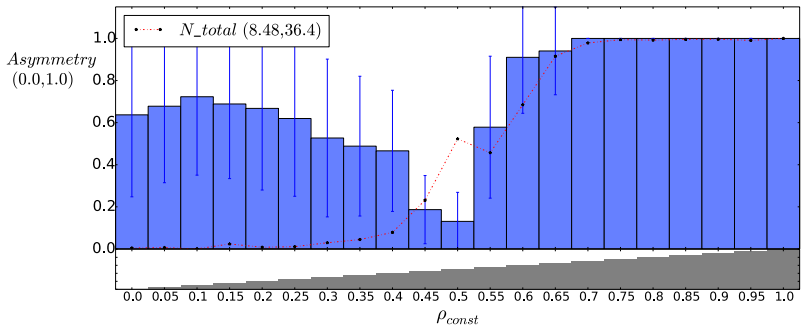

(a)

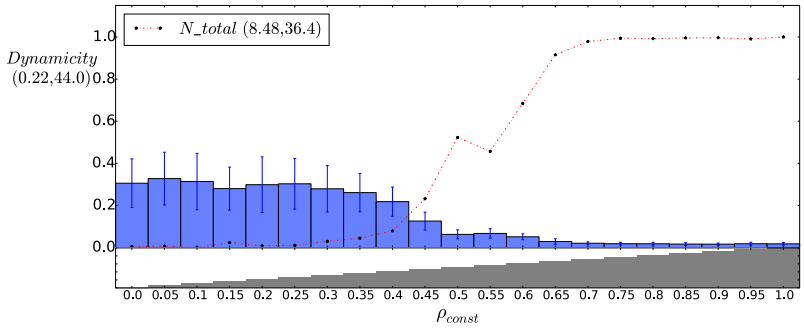

(b)

Figure 27: Asymmetry, dynamicity, and number of nodes for VMC structures with different transfer rates (ρ) in setups with $\omega = 0.1$, $\beta = 10$, $\alpha = 0.9$.

in Fig. 29 are different. For example, Fig. 29(a) shows an unstable decision for assigning the resource to a side which constantly fluctuates between the two sides. The setting of Fig. 29(b) on the other hand never decides on one side during the course of the experiment. In Fig. 29(c), the structure quickly chooses one side to grow by assigning most of the resource to it from the early steps. The example of Fig. 29(d) shows some fluctuations in the amount of resource and a final decision for one of the two sides.

The presented behaviors are a result of the competition for the limited resource that is provided at the root (i.e., R_{root}). Here, we call the assignment of more resource to one side of the structure, a *decision making*. In the following, the influence of R_{root} on the performance of the decision making of the structures is investigated. For that, we used the parameter settings of the experiment of Fig. 29(d) which represents some dynamics with a period of fluctuations and eventually convergence to a decision during the course of the experiment. The *performance* is defined as the difference between the fractions of the resources at the two sides of the structure after a fixed period of time:

$$\text{performance} = |R_L - R_R|/(R_L + R_R)$$

where R_L and R_R are the amount of resource assigned respectively to the left and right sides of the structure after 250 time steps. The *performance* is measured for a set of different values of R_{root}. Every setting is repeated for 9000 independent runs. Fig. 30 shows the median performance of the tested R_{root} values. The inset image shows the performance computed based on the number

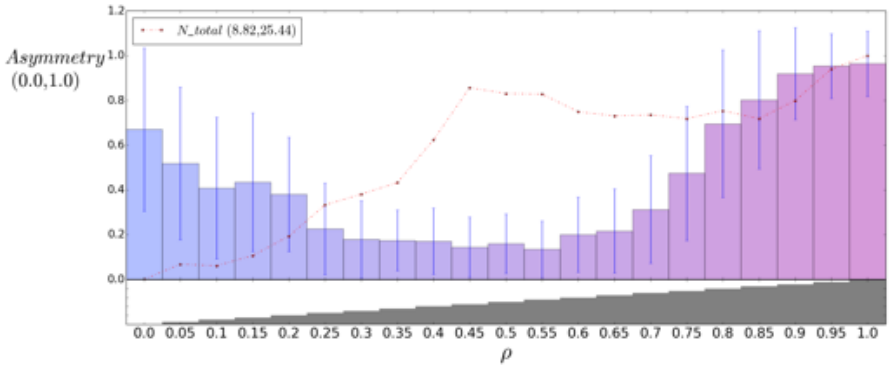

(a)

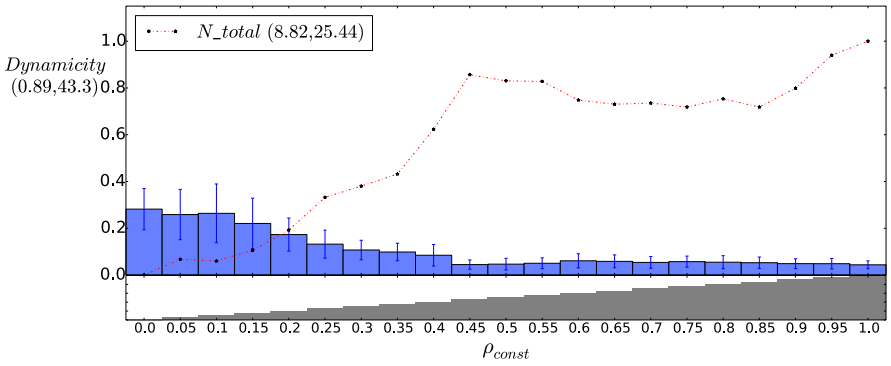

(b)

Figure 28: Asymmetry, dynamicity, and number of nodes for VMC structures for different transfer rates (ρ) in the setups with $\omega = 0.1$, $\beta = 2$, $\alpha = 0.9$.

of nodes at the end of the run instead of the resource values (i.e., the asymmetry measure $|N_L - N_R|/N_{\text{total}}$)).

The Fig. 30 shows very low performances for very low values of R_{root}. The performance moves up by increasing R_{root} and after an optimum value for R_{root} (~ 40 in this case), the performance drops again. The shape of the curve is similar to the generic diagram of system performance over system size for multi-robot systems. The available resource here, R_{root}, is a representative for the system size as it is nearly linearly proportional to the final number of nodes in the structure. The reason for this proportionality is that every non-leaf node holds a constant fraction of the resource (according to the consumption rate).[2] The shape of the performance curve here is similar to multi-robot systems with low interference between the robots, for example due to a body-less (point-like) simulation of robots. That is consistent with the fact that in the current system, we have not implemented any physical effects that could cause physical interactions and potentially lead to interference between the nodes.

As discussed in the theoretical analysis in D2.3, the preconditions for a tendency towards asymmetrical growth in VMC is $\beta > 1$ and $\rho > \frac{1}{n}$ where n is the number of children in every growth event. Both conditions are satisfied in the settings that are used here with $n = 2, \rho =$

[2]The number of non-leaves is linearly proportional to the number of leaves in such a graph, for example, in a 2-branch graph as in here, the number of non-leaves equals to the number of leaves minus one.

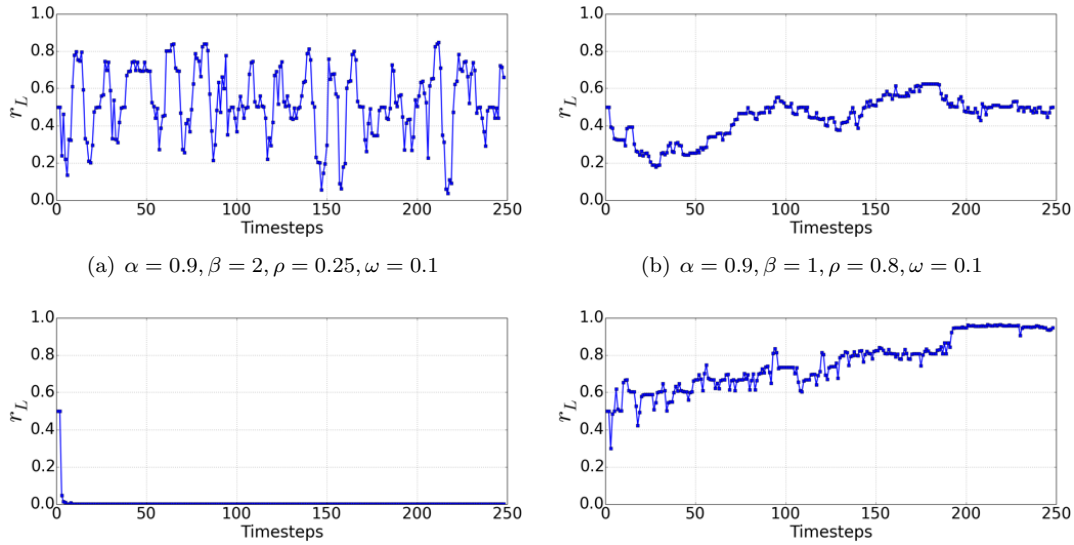

(a) $\alpha = 0.9, \beta = 2, \rho = 0.25, \omega = 0.1$

(b) $\alpha = 0.9, \beta = 1, \rho = 0.8, \omega = 0.1$

(c) $\alpha = 0.9, \beta = 10, \rho = 0.8, \omega = 0.1$

(d) $\alpha = 0.9, \beta = 2, \rho = 0.8, \omega = 0.1$

Figure 29: Example trajectories of $r_L = R_L/(R_L + R_R)$, the fraction of resource assigned to the left side of the structure for different parameter settings. In all examples $R_{\text{root}} = 20$ and all the sensor dependent parameters are set to zero.

$0.8, \beta = 2$. Such a tendency to asymmetry is the positive feedback effect of growth at a branch, either directly or indirectly via the growth of its children, and means further growth at branches with more nodes.

Although the positive feedback leads to reinforcement of asymmetries and higher performance, it has a smaller effect in larger systems compared to smaller ones. The following example helps to explain the reason by comparing two systems of the same symmetrical conditions but different sizes (Fig. 31 illustrates two example systems). Let G be a perfect binary tree of depth r. Assuming an identical successin production of S_{leaf} at all the leaves, the amount of successin at the main left and right branches of the tree after a growth event at the right branch is: $S_L = (2^{r-1})\rho^r S_{\text{leaf}}, \quad S_R = (2^{r-1} - 1 + 2\rho)\rho^r S_{\text{leaf}}$. Hence the proportional successin difference between the left and the right branches is $(S_R - S_L)/(S_R + S_L) = (2\rho - 1)/(2^r - 1 + 2\rho)$. The r is larger in a larger system and therefore such a system has a lower proportional difference. That means a smaller change in the share of the resource reaching each branch, that is, a smaller increase in the possibility of further growth at the right branch. In other words, a change in a large system loses its effectiveness due to a long path between the position of the change and the root. In the same way, in a small system, a growth event makes bigger changes in the distribution of the resource in favor of the larger branch. That leads to a larger positive feedback effect and amplification of growth and facilitates the decision making.

The above mentioned decrease in the positive effect of growth when increasing the system size can explain the lower performance of the larger systems demonstrated in Fig. 30. However, where the system is too small (very small R_{root}), the robustness of the positive feedback effect is reduced. That is because the amplification effect has two sides: a change in the resource distribution and growth in the system can be either due to the positive feedbacks and follows the previous growth events, or it can be due to random fluctuations. Random fluctuations are easily amplified at first and lead to a difference between two sides of the system. But in a system

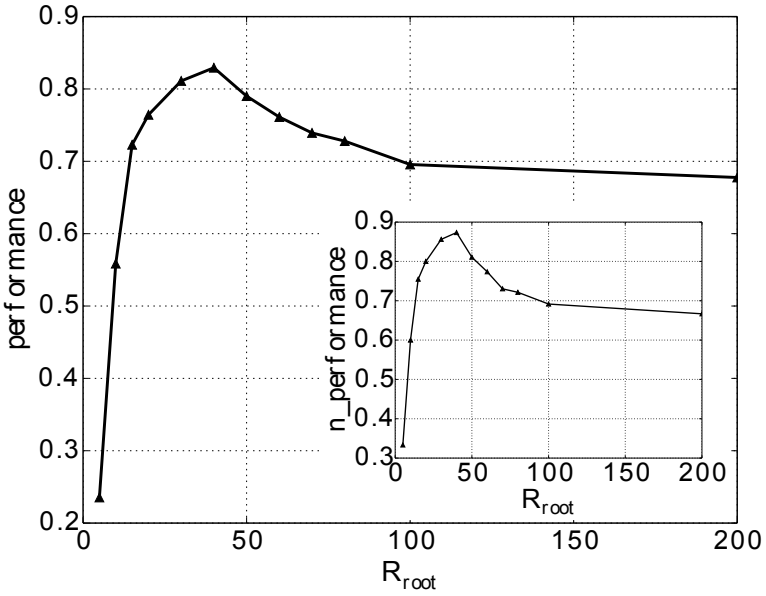

Figure 30: Performance of the decision for one side of the structure with different values of R_{root}. The triangular dots represent median performance of 9000 independent runs for each setting. All the sensor dependent parameters are set to zero. The inset image shows the performance computed based on the number of nodes at the end of the run instead of the resource values.

with a very low amount of resource, the amplification of the first growth events cannot continue for long to produce many new leaves at the majority side. That is because after a few steps, the leaves of the majority branch get too little resource that limits their chance of growth (negative feedback). This puts them in a condition similar to the leaves of the other branch. The next growth events rely mainly on the random fluctuations. In a small system, a single change has a larger effect compared to a large system. In addition, the difference in the number of leaves (options for random growth) at the two sides is small because of the early stop of the majority branch. Therefore, a growth that happens at the minority side due to a random event, is hard to compensate at the majority side. The change at the minority side may be reinforced and win the new majority which is again unstable. This can explain the low performances of very small systems in Fig. 30.

In short, the performance can be seen as the effectiveness of the positive feedback on the asymmetry to lead to a majority decision. For high values of R_{root}, performance is reduced because of the negative contribution of the length of the main branch, whereas for low R_{root}, the negative feedback (limitation of resource) cancels out the positive feedback in early stages and therefore the random fluctuations are the main contributors to the dynamics. The performance peak is where the two effects balance each other.

5.3 Discussion

In the simulation studies, the effects of different parameterizations in dynamical and morphological behaviors of the structures were demonstrated. An interesting example is the effect of transfer rate ρ in the dynamic behavior of the structures. The low values of $\rho < n$ (where n is the number of children of a node) lead to unstable small structures where a small number of

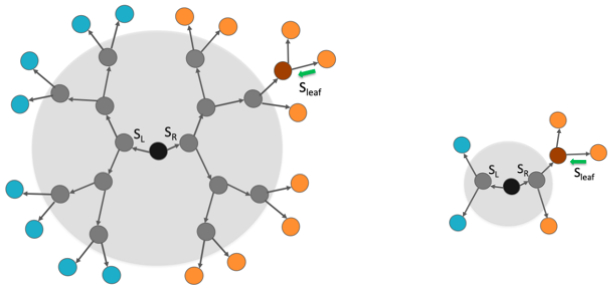

(a) (b)

Figure 31: Two example systems with larger (a) and smaller (b) system sizes.

nodes appear and disappear quickly causing large fluctuations in small structures. With values of $\rho > n$, large and stable structures grow. The change from instability to stability and the explosion of size, makes ρ an interesting parameter with a critical value in $\rho = n$.

The behavior of VMC structure in terms of exploitation vs exploration depends on the parameterizations. The parameters determine the tendency of the structure to explore various options (tendency towards symmetry), to stick to older solutions (asymmetry), or to exploit the current best options. The tendency for current best options is to grow further in the local optima of the environment, that is, growing branches that are currently in favorable regions. Another option is a tendency towards historical choices which is a preference for choices which are made in the past, that is, larger branches. An example is to prefer a branch because it is large, even though it is not any more in a favorable region. The actual decision of the structure depends on both the parameters and the gradients of inputs in the environment.

As discussed in the previous section, the diagram of decision-making performance against the common resource (Fig. 30) in VMC displays similarities with the generic diagram of system performance over system size in multi-robot systems [4]. In general, an analogy can be drawn between the collective process of growth in a VMC structure and a collective decision-making process in a multi-robot or a swarm of agents. As an example, consider a multi-robot decision-making scenario where the robots have two choices. In the beginning, the individual robots choose one of the two possibilities with equal probability because the possible effects of interactions have not yet appeared. Considering the robots as the limited resource of the system, in the beginning, the resource is more or less equally distributed between the two options. Over time, the distribution may change due to fluctuations and interactions between the robots and may lead the system to collectively choose one of the options over the other. The robots in this scenario are both the limited resource that is distributed and the active agents that carry out the distribution via a collective dynamic process. On the other hand, in the VMC system, the concept of distribution of resource is more explicit. The growing system distributes a limited resource between two sides of the system (left/right branches). The resource is in fact expressed as nodes that grow in the structure – recall that a non-leaf node represents a constant amount of resource (according to the consumption rate), a leaf node may cause the growth of new nodes in relation to the amount of resource it holds, and it may be removed if it gets a low amount of resource. In other words, the nodes act both as the representatives of the resource and the active agents carrying out the process of growth and distribution. Similar to the robotic scenario, the system begins with an equal distribution of resource between the two options. Over time and via the fluctuations in the system and interactions between the nodes competing with each other, the distribution may change and eventually reach a state where most of the resource is assigned

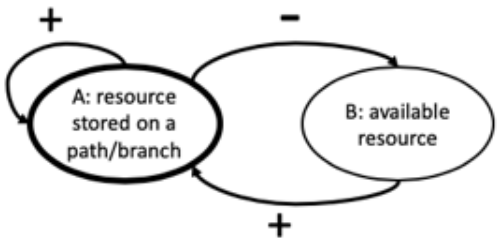

Figure 32: Feedback loops for the resource stored on a path or branch.

to one side of the system for long periods of time.

VMC is inspired by plant morphogenesis and acts on the branching of structures consisting of components that can be added or removed from the system. It implements the concepts of exploration of the environment and reinforcement of favorable branches while losing least favorable ones. Such concepts are shared with self-organized path formation by swarms of mobile agents. As an example, consider the formation of pheromone trails connecting the nest of ants to patches of food. Initially, the individual scout ants that have found a food source lay pheromone in their rather randomly chosen path towards the nest. The pheromone acts as a volatile memory that is stored spatially in environment. It is perceived by other ants and guides them to the food source. The other ants reaching the food, in turn, lay pheromone in their way back to the nest which generates a positive feedback leading to reinforcement of the shortest paths between the nest and the food sources. The role of the mobile agents (e.g., ants) in path formation is fulfilled in VMC by the flows passing through the connection paths that are imposed by the nodes of the directed graph. The positive feedback generated by the reinforcement of favorable paths for the ants is similar to the positive feedback on favorable branches generated by the flows of successin in a VMC system. In both systems, the positive feedback building up the paths collectively is stabilized by the negative feedback. If the food source at the end of a path is limited, it can act as a negative feedback causing the ants to leave the path and form new ones. Another negative feedback which is more of the interest here is the limitation of the number of ants as the limited resource for the structure of the paths. This is similar to the limited resource in VMC that is distributed along the different branches. To make the role of the limited resource in the feedback loops more clear, we can define two variables that influence each other (as demonstrated in Fig. 32): A) the resource that is stored on a path/branch, that is, determines the thickness of a path/branch. B) the available resource which is the resource that is not yet settled somewhere. The feedbacks are considered in respect to A. The positive feedback is quite a direct effect of A on itself, but the negative feedback of A goes through B, that is, the 'available resource,' as shown in Fig. 32. In addition to these effects, the positive feedback in the path formation of ants is influenced negatively by the volatility of the pheromones. In VMC, the positive feedback effect decreases by the negative contribution of the length of branches due to transfer rate $\rho < 1$ (as discussed in the previous section).

6 Conclusions

The results reported in this deliverable D2.4 provide several essential solutions for our current and potential future bio-hybrid developments. Mostly we report continued efforts that were started before and that provide the methodology to achieve the project's objectives. This is the case, for example, for our algorithms for bio-hybrid growth, that were developed iteratively in different types of plant-robot setups. We had started from simple setups and have increased the complexity step by step. Also, our work on the VMC was started almost at the beginning of the project. The study here shows our gathered experience and knowledge about the VMC in a mature form. The VMC is applied in *flora robotica* in different forms but is also a contribution to the community and it will most likely be applied also in the future beyond this project. Applications of the Phytosensor have been constantly studied and advanced. However, the complexity of plant anatomy, the lack of structures analogous to nervous systems, and the lack of a full holistic understanding of plants, cause that plant electric potentials are challenging to apply in bio-hybrid systems. Further improvements in experimental methodology and data analysis could make it possible to apply the Phytosensor for monitoring of environments and plant physiology. The presented detection of plant damage by analyzing Phytosensor data is ready to use in our *flora robotica* experiment setup.

In conclusion, we note that this deliverable D2.4 is one of the first documents that extensively and comprehensively reports on algorithms for plant bio-hybrid growth and plant affection of bio-hybrids. Especially the chapter on algorithms for bio-hybrid growth may be useful in future research on bio-hybrid plant systems. The presented data from our plant-electrophysiological experiments can be of similar use in future research, especially to show the potential of this technology. Similarly for the VMC, as said, it will be a useful tool across different domains.

References

[1] Ronald C. Arkin and Magnus Egerstedt. Temporal heterogeneity and the value of slowness in robotic systems. In *2015 IEEE International Conference on Robotics and Biomimetics (ROBIO)*, pages 1000–1005. IEEE, 2015.

[2] Francisco Carrapiço. Azolla as a superorganism. its implication in symbiotic studies. In *Symbioses and stress*, pages 225–241. Springer, 2010.

[3] Monica Gagliano, Vladyslav V. Vyazovskiy, Alexander A. Borbély, Mavra Grimonprez, and Martial Depczynski. Learning by association in plants. *Scientific Reports*, 6:38427, 2016. ISSN 2045-2322. doi: 10.1038/srep38427. URL http://www.nature.com/articles/srep38427.

[4] Heiko Hamann. Superlinear scalability in parallel computing and multi-robot systems: Shared resources, collaboration, andnetwork topology. In Mladen Berekovic, Rainer Buchty, Heiko Hamann, Dirk Koch, and Thilo Pionteck, editors, *Architecture of Computing Systems – ARCS 2018*, pages 31–42, Cham, 2018. Springer International Publishing. ISBN 978-3-319-77610-1.

[5] Danillo Roberto, João Paulo, Gustavo Francisco, Rosalin Saraiva, Gustavo Maia, and Optimum-path Forest. Automatic classification of plant electrophysiological responses to environmental stimuli using machine learning and interval arithmetic. *Computers and Electronics in Agriculture*, 145:35–42, 2018. ISSN 0168-1699. doi: 10.1016/j.compag.2017.12.024. URL https://doi.org/10.1016/j.compag.2017.12.024.

[6] William B. Sanders. A feeling for the superorganism: expression of plant form in the lichen thallus. *Botanical journal of the Linnean Society*, 150(1):89–99, 2006.

[7] Thomas D. Seeley. The honey bee colony as a superorganism. *American Scientist*, 77(6): 546–553, 1989.

[8] Chao Song, Xiao-Huang Qin, Qiao Zhou, Zi-Yang Wang, Wei-He Liu, Jun Li, Lan Huang, Yang Chen, Guiliang Tang, Dong-Jie Zhao, et al. PlantES: A plant electrophysiological multi-source data online analysis and sharing platform. *Applied Sciences*, 8(11):2269, 2018. doi: 10.3390/app8112269.

[9] Mostafa Wahby, Mary K. Heinrich, Julian Petzold, Igor Kuksin, Payam Zahadat, Thomas Schmickl, Phil Ayres, and Heiko Hamann. Robotic sensing and stimuli provision for guided plant growth. *Journalof Visualized Experiments*, 2019. (conditionally accepted).

[10] David Sloan Wilson and Elliott Sober. Reviving the superorganism. *Journal of theoretical Biology*, 136(3):337–356, 1989.